Technische Universität München
Ingenieurfakultät Bau Geo Umwelt
Lehrstuhl für Astronomische und Physikalische Geodäsie
Univ.-Prof. Dr.techn. Mag.rer.nat. Roland Pail

Tropospheric Correction Modeling in SAPOS Reference Network under Large Height Difference Condition

Chengyue Qian

Master's Thesis

Master's Course in Earth Oriented Space Science and Technology

Supervisor(s): Univ.-Prof. Dr.phil.nat. Urs Hugentobler
Institut für Astronomische und Physikalische Geodäsie, TUM

Date of Submission: April 15, 2016

Declaration

This thesis is a presentation of my original research work. Wherever contributions of others are involved, every effort is made to indicate this clearly, with due reference to the literature, and acknowledgement of collaborative research and discussions.

Munich , ……... (date) …..……(Author's signature)

Acknowledgements

I would like to thank all the people who are involved in the ESPACE Double Degree program and who help and support me during my master studies.

First and foremost, I would like to express my deepest gratitude to my supervisor Professor Urs Hugentobler for his constant encouragement and patient guidance through my thesis work. Professor Hugentobler not only gave me ingenious ideas, provided me valuable advices, but also taught me solve practical difficulties even sacrificing his lunchtime. His kindness and friendliness have greatly impressed me and will certainly be my lifelong memory.

I would like to appreciate my supervisor Professor Yongjun Zhang in Wuhan University for offering me the opportunity to study here. I benefit a lot from his the enlightenment and cultivation on scientific research for me.

I would like to appreciate Dr. Christof Völksen from BAdW and Mr. Martin Freitag from LDBV. They shared me with valuable ideas and gave me generous support. Many thanks to Mr. Freitag, for his laborious preparation of SAPOS data.

I would also like to thank all the lecturers and staff of ESPACE Master's Program for such an international prestigious study program. I really benefit a great deal from the courses and activities. Thanks for my classmate and my Wuhan University fellows for sharing unforgettable experience abroad.

Last but not least, my gratitude to my parents for their eternal love and unconditional support.

Abstract

Nowadays tropospheric delay still remains a major error source in GNSS positioning. To mitigate tropospheric refraction effect, various empirical tropospheric models together with mapping functions have been built. Approximately 90% tropospheric delay comes from hydrostatic component of troposphere which can be well corrected by empirical models. However, the remaining wet component is highly variable within spatial and temporal domain, resulting in decimeters level error in the zenith direction. Hence, it is very difficult to satisfy the demands of various high precision applications.

In the past 20 years, many regional GNSS reference networks have been constructed. Therefore, a regional tropospheric delay model could be established by exploiting resolved tropospheric delay at reference station. Tropospheric delay is largely influenced by height factor and shows different characteristics in the horizontal and height directions. In mountainous areas, conventional models might result in great unmodeled systematic bias in case of large height difference.

This thesis aims to provide a solution to regional troposphere modeling for undulating areas with large height variation. For this purpose, four major work have been done: (1) Investigation of the correlation between tropospheric delay and station height; (2) Using Least Square Collocation (LSC) method for parameter estimation and presenting a method to estimate the covariance parameters; (3) Proposing a horizontal-height delay decomposition tropospheric model; (4) Evaluation of the effectiveness of established model with respect to the network configuration, i.e., number, baseline length and distribution of reference stations.

Key words: GNSS, tropospheric model, least square collocation, horizontal-height delay decomposition model

Table of Contents

List of Figures

List of Tables

Chapter 1 Introduction

1.1 Background

The Global Navigation Satellite System (GNSS) is a satellite constellation that emits radio-frequency signals to provide accurate position, velocity and time (PVT) information for users with global coverage. While GNSS was initially developed for military purpose, it has made tremendous development in civil fields over the past few decades. More specifically, there is a rapid growing demand for real-time, high-precision positioning (decimeter to millimeter level) in many applications at present time and in the foreseeable future, to name but a few, geodetic surveying, deformation monitoring, intelligent transportation and precise farming.

However, many error sources diminish the accuracy of GNSS measurements, among which tropospheric refraction is considered as the ultimate accuracy–limiting factor for GNSS–based geodetic applications (Dach et al., 2007). When radio signals propagate through the atmosphere, they would suffer refraction from two different layers of atmosphere, namely the ionized ionosphere and the neutral troposphere. The troposphere is a non–dispersive medium for radio-frequency GNSS signals. Hence, tropospheric refraction is independent of signal frequencies and not possible be eliminated by combination of two separate frequency signals like ionospheric refraction. The neutral propagation delay can be divided into two components: the hydrostatic component caused by dry gases and the wet component by water vapor in the air. The hydrostatic delay accounts for approximately 90% of the total delay and it varies smoothly in both spatial and temporal domain, and it can be well modeled as a function of temperature, pressure and humidity. Nevertheless, the wet delay is highly variable with space and time, making it hard to model. The troposphere has a great influence on the accuracy of positioning, especially on the height component. Consequently, extensive efforts have been devoted to the reduction of its impact. Generally, there are four categories of techniques to handle with this problem.

The first category technique is using meteorological radiosonde and water vapor radiometer (WVR) to estimate tropospheric delay. A radiosonde is carried into the atmosphere by balloon and measures various

meteorological parameters such as altitude, pressure, temperature and relative humidity. Then by ray-tracing technique the parameters can be converted to tropospheric delay. Unlike radiosonde, a WVR is a gound-based passive instrument that measures the energy emitted from water vapor content and then transforms to wet path delay with interpretation algorithms. It should be noted WVR only works for the wet component of tropospheric delay. This category of techniques is able to provide highest possible accuracy estimation at current stage, even under severe convective weather. However, the high cost of instruments and limited spatial and temporal resolution are the major drawbacks of this technique. Therefore it is often used for scientific research as ground truth to build empirical models and assess other techniques.

The second category is using empirical tropospheric models together with mapping functions, e.g., Saastamoinen model, Hopfield model, Niell Mapping Function (NMF), Vienna Mapping Function (VMF) and Global Mapping Function (GMF). These models are mainly established analytically based on long term (from a few years up to decades) meteorological observations of atmosphere, and able to estimate the hydrostatic delay with high accuracy. However, due to the high variability of water vapor content, there stills remains large residuals in the wet delay correction. To a large extent, the empirical models provide correction for tropospheric delay.

The third category is to take tropospheric wet delay as unknown parameters in the process of positioning. The wet delay is modeled as stochastic process and estimated by least squares or Kalman filter methods. In scientific GNSS processing software like Bernese and GAMIT, least squares estimation is applied: for a given interval, the zenith delay is considered as constant; taking the empirical model derived zenith hydrostatic delay as an a priori value, and then estimating wet delay from the residuals, finally obtaining the zenith total delay. Extensive researches have proven that the accuracy of estimated zenith wet delay is comparable to the one derived from WVR with bias less that 1cm. Hence, it seems that this technique is the best way to deal with tropospheric refraction effect.

The fourth category is the RTK technique which employs the spatial correlation of atmospheric error. Conventional RTK technique is in essence relative positioning technique which involves with two receivers,

the reference station with known position and the rover to be positioned. The baseline between the rover and reference station is usually only a few kilometers. In general, all the spatially error such as orbit error, tropospheric and ionospheric refraction are quite similar and could be eliminated by differencing processing, remaining infinitesimal residuals. However, the maximum baseline length is the limited to 10km to fulfill the spatial correlation assumption.

Network RTK is an emerging technique which greatly enlarges the working range of conventional RTK up to hundred kilometer level. This technique seems to be a combination from some of the above categories. In the past decades, many regional GNSS reference networks have been constructed, to name but a few, the Canadian Active Control System (CACS), the Continuously Operating Reference Stations (CORS), the Satellite Positioning Service of the German State Survey (SAPOS) and Australian Regional GNSS Network (ARGN). Except for scientific functions like geodetic datum determination and crustal deformation monitoring, these fundamental infrastructures can also provide atmospheric errors correction based on continuous observations at the spatially distributed reference stations. The atmospheric errors at the reference stations can be estimated as unknown parameters in data processing and then built as a regional error model. Hence, the spatially correlated errors of the rover within the network area coverage are available, thus increasing the accuracy of positioning. Obviously, the accuracy of error model is the key factor for the performance of rover positioning, since it determines how well the spatial error could be corrected from the observations. And various methods have been proposed and implemented in the current Network RTK systems.

1.2 Motivation and Objectives

The theoretical basis of the error modeling techniques is the correlation and homogeneity of atmospheric errors in spatial distribution. However, the tropospheric refraction is highly affected by the station height: not only due to the different total path, but the discrepancy of meteorological conditions like pressure, temperature and relative humidity. Hence, if there exist large height difference between the reference station and the rover, the spatial correlation would be jeopardized, resulting in degraded positioning results.

CHAPTER 1 INTRODUCTION

Due to the influence of height, the tropospheric delay has significant different characteristics in the horizontal and height direction. Existing Network RTK error modeling methods do not take much focus on the height factor, and few researches are aiming at this problem. The reasons might be twofold: the first one is that most reference networks are constructed in plain areas which are more suitable for human inhabit, while mountainous areas are with less residents. And the second reason is that the requirements for high precision positioning are not demanding in the past decades.

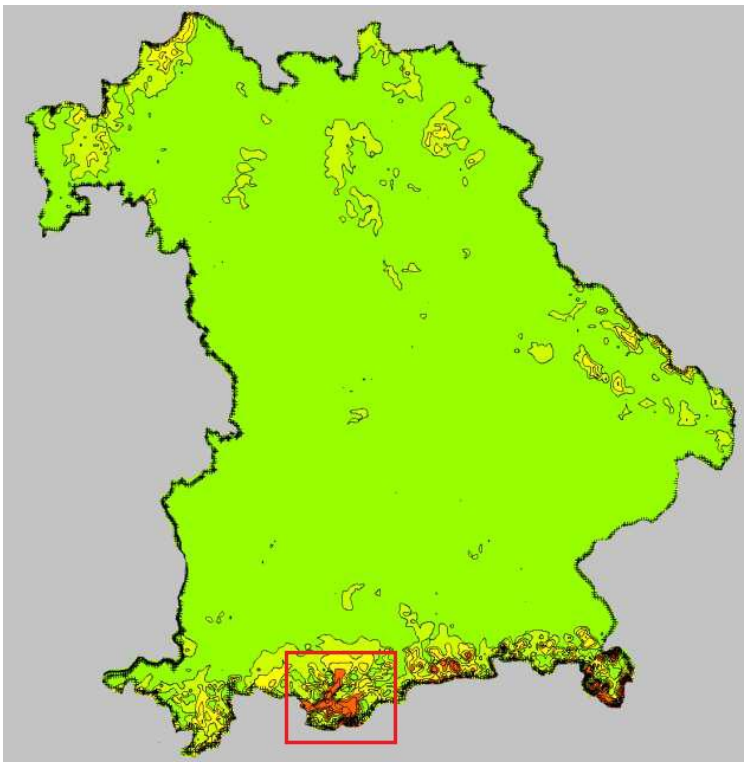

Figure 1.1 Height difference with SAPOS reference stations (modified after SAPOS website)

This thesis is supported by Landesamt für Digitalisierung, Breitband und Vermessung Bayern (LDBV) to investigate the above problem existing in the Garmisch-Patenkirchen area. The Garmisch-Patenkirchen area is in the Ester Mountains range with highly undulating terrain. The figure 1.1 illustrates the height difference of surface with respect to SAPOS reference stations. The green indicates the height difference at 300m, while red indicates greater than 600m, marked by the red rectangle. The reference station 0285 (Garmisch) locates in the summit of Wank mountain up to 1780 meters above mean sea level. When the rover is in the valley, the Network RTK service provided by SAPOS would introduce large systematic bias

to the correction of tropospheric delay, degrading positioning error in height component up to 10cm.

The main purpose of this thesis is to provide a solution to the regional tropospheric error modeling for the areas with large height variation. The major objectives are including the following three aspects. The first objective is to investigate the tropospheric delay derived from GNSS processing, especially the relationship between the magnitude and height, laying foundations for the further study. The second one is to implement various existing region tropospheric error models, and assess the performance of them. The third one is to develop a new model which takes account for the influence of height factor, with detailed performance assessment with respect to baseline length, reference numbers and distribution.

1.3 Structure of the thesis

The thesis is composed of five chapters and each of them will be organized as follows.

The first chapter gives a brief introduction of the whole thesis, including the background information, motivation and major objectives of this research.

The second chapter provides the theoretical fundamentals involved in this thesis. It consists of three parts: (1) the basic equation and methods of GNSS processing; (2) the troposphere characteristics and its impacts on signal propagation as well as its modeling; (3) the basis of Network RTK technique and classical error interpolation methods.

The third chapter illustrates the workflow briefly, and focuses on the Least Squares Collocation method and detailed description of the proposed new model, i.e., the horizontal-altitude delay decomposition model.

The fourth chapter presents results of experiment, including the performance of difference models, and the influence of network configuration.

The last chapter makes conclusions on the research and discusses further studies concerning the topic.

Chapter 2 Theoretical Background

In this chapter, the theoretical basis related to the thesis is illustrated. Firstly, the basic GNSS observations are briefly introduced. Secondly, the characteristics of troposphere are presented, i.e., its vertical structure, composition and effects on signal propagation. Afterwards, various widely used empirical models and mapping functions are generally described. Thirdly, an overview of Network RTK technique is given and the emphasis is laid on the interpolation methods for correction generation.

2.1 GNSS Basis

GNSS is based on an ancient technique called trilateration which determines an unknown position by measuring its distance to a few points with known coordinates. In GNSS, a receiver measures its distance to simultaneously observed four or more satellites from Time of Arrival (TOA) and calculates the position of these satellites from the navigation message demodulated from the signals. Through the positions of the satellites and measured distances, the position of the receiver could be determined. Existing systems with full operational capability (FOC) includes the GPS of USA and GLONASS of Russia while European Galileo and Chinese BeiDou are still in development.

2.1.1 Basic Observations

The GNSS satellites continuously broadcast L-band radio frequency signals in two or more frequencies used for positioning and timing. The basic observations are including code pseudoranges, carrier phase and Doppler measurements.

The code pseudorange is deduced from the signal travel time from a satellite to the receiver, i.e., the difference between signal reception time at the receiver and the emission time at the satellite. The carrier phase is much more precise that code pseudorange. It measures the phase difference between receiver generated carrier and the carrier received from satellite at the reception time. However, it is ambiguous measurement since only the fractional part of phase is measured and the initial integer number cycles of phase difference remains unknown. And this integer number is called ambiguity. The Doppler shift measurement which is not popularly used in high precision applications and is not discussed further.

CHAPTER 2 THEORETICAL BACKGROUND

The code pseudorange and phase observations are suffered from various systematic errors including satellite orbits, satellite and receiver clocks, tropospheric and ionospheric refraction, antenna phase centre offset and variations, relativistic effects and multipath effects. Besides, with respect to reference networks for high precision applications, more base station related errors should be taken into account like solid earth tide, pole tide, ocean tide and atmospheric tide loading as well as plate tectonic motion. For simplicity and emphasis, only the most important measurement errors would be modeled in the following basic observation equations (Xu, 2007):

$$P = \rho + c(dt_r - dt^s) + T + I + \varepsilon_P \tag{2.1a}$$

$$\Phi = \rho + c(dt_r - dt^s) + T - I + \lambda N + \varepsilon_\Phi \tag{2.1b}$$

where

P: the code pseudorange observation

Φ: the carrier phase observation

ρ: the geometric distance between the satellite and receiver

c: the speed of light

dt_r: the receiver clock error

dt^s: the satellite clock error

T: the tropospheric delay error

I: the ionospheric delay error

λ: the wavelength of carrier

N: the carrier phase initial ambiguity

$\varepsilon_P, \varepsilon_\Phi$: the receiver code and carrier noise

In equation 2.2, the ambiguous nature of phase observation is depicted by the integer ambiguity term N. And it is also obvious that the ionospheric error has the same magnitude but opposite signs for the code and phase observations. This is the result of different effects of ionosphere on code and carrier wave: the code observation is delayed while the carrier phase is advanced.

2.1.2 Forming Difference

The differencing technique is commonly used to reduce the measurement errors. The most important ones are single difference and double difference, and the geometry is illustrated in Figure 2.1.

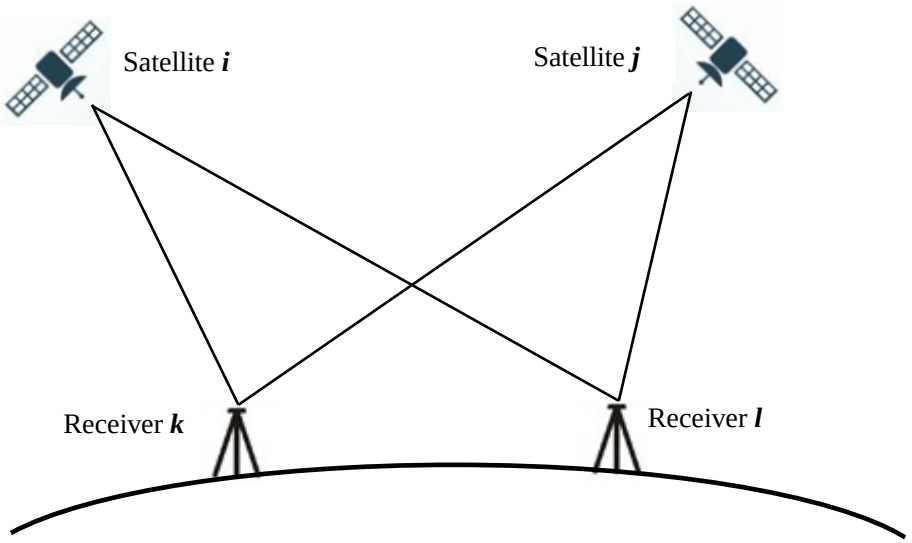

Figure 2.1 Observation differencing geometry

Single Difference

Single difference includes two categories. The first one is the difference of the simultaneous observations of a common satellite ***j*** to two receivers ***k*** and ***l***, and the second is the difference from two satellites ***i*** and ***j*** with a common receiver ***k***. For the first category, namely two receivers and one satellite, the differencing equation could be expressed:

$$\Delta P_{kl}^{j} = \Delta\rho_{kl}^{j} + c\Delta dt_{kl} + \Delta T_{kl}^{j} + \Delta I_{kl}^{j} + \varepsilon_{P,kl}^{j} \tag{2.2a}$$

$$\Delta \Phi_{kl}^{j} = \Delta\rho_{kl}^{j} + c\Delta dt_{kl} + \Delta T_{kl}^{j} - \Delta I_{kl}^{j} + \lambda\Delta N_{kl}^{j} + \varepsilon_{\phi,kl}^{j} \tag{2.2b}$$

the symbol Δ denotes the differencing operator, the subscripts ***k*** and ***l*** denote two receivers, and the superscript ***j*** denotes the satellites. It is clear that the satellite clock error is eliminated. Besides, for short baseline up to a few kilometers, the atmospheric path delay could be largely reduced. In a flat area, it is true that atmosphere conditions are similar within short distance up to ten kilometers. However, it should be noted that in the special case where two receivers locate with large height difference, the similar atmosphere condition would be violated due to the height, thus the differencing technique would not be

effective. Similarly, for two satellites and one receiver, the differencing equation reads as follows with the cancellation of receiver clock error.

$$\Delta P_k^{ij} = \Delta\rho_k^{ij} + c\Delta dt^{ij} + \Delta T_k^{ij} + \Delta I_k^{ij} + \varepsilon_{P,k}^{ij} \quad (2.3a)$$

$$\Delta \Phi_k^{ij} = \Delta\rho_k^{ij} + c\Delta dt^{ij} + \Delta T_k^{ij} - \Delta I_k^{ij} + \lambda\Delta N_k^{ij} + \varepsilon_{\phi,k}^{ij} \quad (2.3b)$$

Double Difference

Double difference could be obtained just a step further by forming difference of the single difference observations, i.e., two satellites and two receivers:

$$\nabla\Delta P_{kl}^{ij} = \nabla\Delta\rho_{kl}^{ij} + \nabla\Delta T_{kl}^{ij} + \nabla\Delta I_{kl}^{ij} + \varepsilon_{P,kl}^{ij} \quad (2.4a)$$

$$\nabla\Delta \Phi_{kl}^{ij} = \nabla\Delta\rho_{kl}^{ij} + \nabla\Delta T_{kl}^{ij} - \nabla\Delta I_{kl}^{ij} + \lambda\nabla\Delta N_{kl}^{ij} + \varepsilon_{\phi,kl}^{ij} \quad (2.4b)$$

where $\nabla\Delta$ denotes double differencing operator. The satellite and receiver clock errors are both eliminated. The remaining tropospheric and ionospheric errors are characterized as spatially correlated errors whose magnitude depends on baseline length. Double difference technique greatly reduces the measurement error and serves as the theoretical basis of RTK technique.

2.1.3 Linear Combinations

Based on the code pseudorange and carrier phase observations from two frequencies, e.g., L1 and L2, linear combinations of observations could be formed, which are advantageous for different GNSS application. The most commonly used ones are ionosphere-free combination, geometry-free combination and wide-lane combination (Hofmann, 2001).

Ionosphere-free Combination

The ionosphere-free combination takes advantage of the frequency-dependency of ionospheric delay. It removes the first-order ionospheric effect which accounts for 99% of the total effect. It should be noted that the ambiguity of the ionosphere-free combination is not necessarily an integer value, but it makes the estimation of tropospheric delay much easier. Therefore, it is widely used in GNSS processing if dual frequency observations are available. The ionosphere-free combination could be expressed as:

$$P_{IF} = \frac{f_1^2}{f_1^2 - f_2^2} P_1 - \frac{f_2^2}{f_1^2 - f_2^2} P_2 = \rho + c(dt_r - dt^s) + T + \varepsilon_{P,IF} \quad (2.5a)$$

$$\Phi_{IF} = \frac{f_1^2}{f_1^2 - f_2^2} \Phi_1 - \frac{f_2^2}{f_1^2 - f_2^2} \Phi_2 = \rho + c(dt_r - dt^s) + \frac{\lambda_1 N_1 - \lambda_2 N_2}{f_1^2 - f_2^2} + T + \varepsilon_{\Phi,IF} \quad (2.5b)$$

Geometry-free Combination

The geometry-free combination is simply the difference between observations in two frequencies. It eliminates the geometry related terms such as satellite-receiver distance, satellite and receiver clock errors and tropospheric delay error, only remaining ionospheric term. Hence, this combination is mainly used to estimate the ionospheric delay and build ionosphere models. It is notable that the so-called Differential Code Bias (DCB) should be taken into consideration in the estimation. The geometry-free combination could be formed as:

$$P_{GF} = P_1 - P_2 = (1 - \frac{f_1^2}{f_2^2}) I_1 + \varepsilon_{P,GF} \quad (2.6a)$$

$$\Phi_{GF} = \Phi_1 - \Phi_2 = -(1 - \frac{f_1^2}{f_2^2}) I_1 + \lambda_1 N_1 - \lambda_2 N_2 + \varepsilon_{\Phi,GF} \quad (2.6b)$$

Wide-lane Combination

The wide-lane combination is used to create carrier phase observation with long wavelength. The formed wide-lane wavelength is up to 86.2cm and this preferable property greatly enhances the ambiguity resolution as well as cycle slip detection in data preprocessing.

$$P_{WL} = \frac{f_1}{f_1 + f_2} P_1 + \frac{f_2}{f_1 + f_2} P_2 \quad (2.7a)$$

$$\Phi_{WL} = \frac{f_1}{f_1 - f_2} \Phi_1 - \frac{f_2}{f_1 - f_2} \Phi_2 \quad (2.7b)$$

2.2 Troposphere Modeling

When GNSS signals propagate through the atmosphere, their direction and velocity would be changed by different medium. This phenomenon is referred as refraction which affects the transmission time. And this time delay or advance would result in measurement error in the observations, namely, atmospheric error. Different layers of atmosphere could be identified based on physical and chemical properties. Possible subdivision schemes are given in Figure 2.2 (Seeber, 2003). According to physical characteristics of signal

propagation, the atmosphere could be divided into two layers: ionosphere and troposphere. In this section, the effects of troposphere are introduced since it is the core of the thesis.

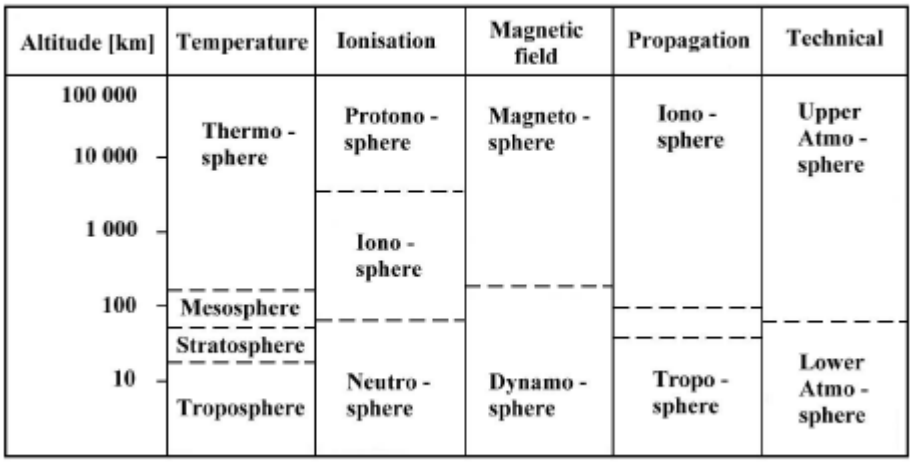

Figure 2.2 Possible subdivision schemes of Earth’s atmosphere (Seeber, 2003)

2.2.1 Overview

In GNSS domain, the troposphere actually refers to the neutral atmosphere which extends from the Earth surface to an altitude of 50km, including troposphere, tropopause and stratosphere from low to high. The reason for the convention is that the troposphere contains approximately 75% of the atmosphere's mass and 99% of its water vapor and aerosols (Wikipedia, 2016); hence it dominates the neutral atmospheric propagation delay. The neutral troposphere is a non-dispersive medium for L-band radio frequency, and it has the same impact on L1 and L2 measurements, and also for code and phase measurements.

As for the chemical composition, the troposphere is composed of dry air and water vapor. Dry air is mainly composed of three gases: nitrogen, oxygen and argon. Together, these three gases make up more than 99.9% of the mass of dry air (Wikipedia, 2016). Water vapor is water in its gaseous state and extremely important to the weather and climate. All of the water vapor evaporating from the Earth surface eventually returns as precipitation. It is highly variable both spatially and temporally. Accordingly, the tropospheric path delay could be modeled as two parts: the hydrostatic delay and the wet delay. It should be noted that the hydrostatic component not only models the dry air but also the water vapor in hydrostatic equilibrium

based on ideal gas law. The hydrostatic component contributes approximately 90% of the total delay and could be modeled with an accuracy of better than 1%. At the sea level, the hydrostatic delay in the zenith direction is about 2.3m under standard atmospheric condition (Parkinson, 1996). However, the remaining 10% wet component could not be modeled accurately due to its dynamic nature.

In theoretical research, the tropospheric delay TD is represented with the refractive index n (Dach et al., 2007):

$$TD = \int (n-1)\, ds = 10^{-6} \int N\, ds \tag{2.8}$$

The integration is taken along the signal transmitting path through the atmosphere. The refractive index anomaly $n-1$ is usually scaled and replaced by refractivity N for simplification. The refractivity is not a constant along the signal path and it varies with altitude. More specifically, it is a function of pressure, temperature and relative humidity. The N could be divided into the hydrostatic and wet component, N_H and N_W respectively, hence

$$TD = TD_H + TD_w = 10^{-6} \int N_H\, ds + 10^{-6} \int N_W\, ds \tag{2.9}$$

Generally, the tropospheric delay is modeled in the zenith direction, namely zenith tropospheric delay (ZTD). And the delay in arbitrary direction, called the slant tropospheric delay (STD), could be derived based on a mapping function. The scheme of mapping is illustrated in Figure 2.3, without showing propagation path bending effect.

Similarly, the mapping function itself could also be divided to the hydrostatic and wet mapping functions and equation 2.16 becomes:

$$STD(\varepsilon) = m_H(\varepsilon) ZTD_H + m_W(\varepsilon) ZTD_W \tag{2.10}$$

where the $m_H(\varepsilon)$, $m_W(\varepsilon)$ is the hydrostatic and wet mapping function with satellite elevation angle ε, and the ZTD_H, ZTD_W is the zenith hydrostatic and wet delay. Obviously, the two key issues are zenith delay and mapping function modeling.

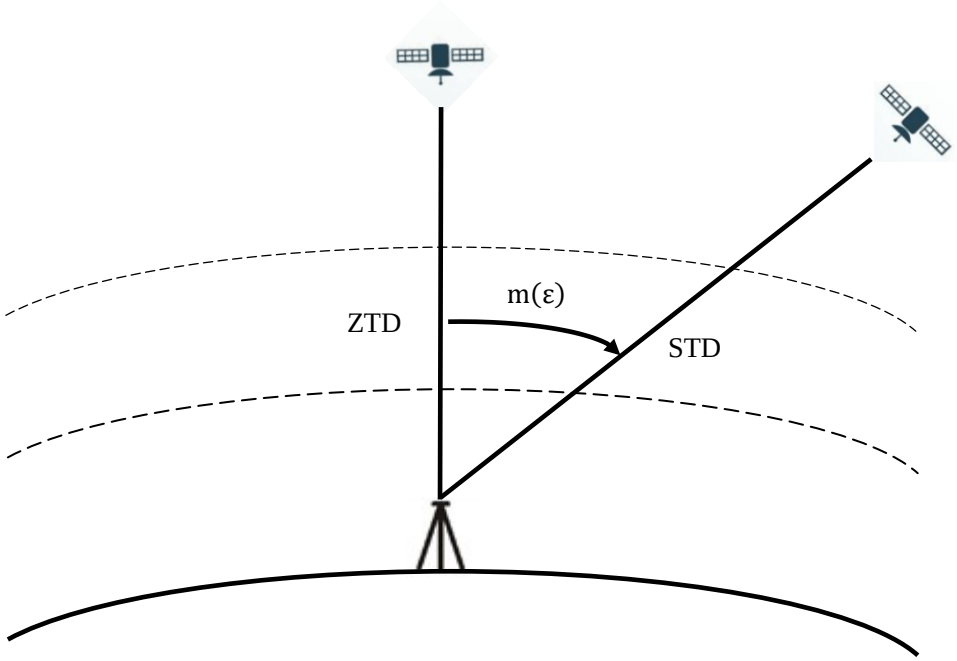

Figure 2.3 Scheme of mapping function

2.2.2 Empirical Delay Models

The refractivity is a function of pressure, temperature and relative humidity. However, it is difficult to measure the refractivity along the propagation path. Therefore, various empirical models are developed to build a connection between the ZTD and the surface meteorological parameters. Here the most widely used two models Saastamoinen Model and Hopfield Model are introduced. These models could provide a priori value for estimation of tropospheric parameters in GNSS processing.

Saastamoinen Model

The Saastamoinen model was derived theoretically based on ideal gas law and it assumes gravity acceleration as a function of height with hydrostatic equilibrium (Saastamoinen, 1973). The tropospheric delay could be expressed as:

$$TD = \frac{0.002277}{\cos z}\left(P + \left(\frac{1255}{T} + 0.05\right)e - \tan^2 z\right) \tag{2.11}$$

Where the atmospheric pressure P and partial water vapor pressure e are in millibar unit, T is the Kelvin temperature, z is satellite zenith angle. And these three parameters at the station with height h are generally derived based on standard atmosphere model:

$$P = P_0 \cdot (1 - 0.0000226 \cdot (h - h_0))^{5.225} \quad (2.12a)$$

$$T = T_0 - 0.0065 \cdot (h - h_0) \quad (2.12b)$$

$$Rh = Rh_0 \cdot exp\,(-0.0006396 \cdot (h - h_0)) \quad (2.12c)$$

$$e = Rh \cdot exp\,(-37.2465 + 0.213166T - 0.000256908T^2) \quad (2.12d)$$

The reference height h_0 is taken as 0m, and in standard atmosphere model:

$$P_0 = 1013.25\,mb,\ T_0 = 18℃,\ Rh = 50\% \quad (2.13)$$

Later an updated version of Saastamoinen Model was given by Baueršíma with height related correction terms B and δ_R along with the lookup table (Dach et al., 2007):

$$TD = \frac{0.002277}{cos\,z}\left(P + \left(\frac{1255}{T} + 0.05\right)e - B\,tan^2\,z\right) + \delta_R \quad (2.14)$$

Hopfield Model

Hopfield Model is a quadratic form model established from radiosonde meteorological data on the basis of hydrostatic equilibrium condition (Hopfield, 1969). And it assumes constant gravity acceleration. It models the hydrostatic refractivity N_H and wet refractivity N_W separately by fourth-degree function of height h:

$$N_H = N_{H,0}(\frac{h_H - h}{h_H})^4 \quad (2.15a)$$

$$N_W = N_{W,0}(\frac{h_W - h}{h_W})^4 \quad (2.15b)$$

where $N_{H,0}$ and $N_{W,0}$ are the refractivity of hydrostatic and wet component on the surface, and h_H and h_W are the height parameters obtained by a least-squares fit to observed data, which define the effective thickness of effective troposphere. And the hydrostatic thickness h_H is taken in km while h_w is locally dependent:

$$h_H = 40.082 + 0.14898T_c \quad (2.16)$$

By integration, the zenith delay could be obtained:

$$ZTD_H = \frac{10^{-6}}{5}N_H h_H \quad (2.17a)$$

$$ZTD_W = \frac{10^{-6}}{5}N_H h_H \quad (2.17b)$$

A modified version of Hopfield models (Goad & Goodman, 1974) have been derived by introducing length of position vectors rather than height:

$$N_i = N_{i,0}\left(\frac{r_i - r}{r_i - R_E}\right)^4 \tag{2.18}$$

where $r_i = R_E + h_i,\ r = R_E + h$ and i denotes the hydrostatic or wet component and R_E is the Earth radius. The solution of integration results in more versions of Hopfield Model and will not be discussed here.

2.2.3 Mapping Functions

Mapping function describes the relationship between the zenith delay and the slant delay. The simplest mapping function could be the cosecant of elevation angle. However, due to both the curvature of Earth and the bending of signal propagation path, this mapping function results in large deviation in low elevation case. Thus more sophisticated mapping functions have been developed to deal with this impact.

Marini Mapping Function

The Marini Mapping Function (Marini, 1972) is introduced because it lays the foundation for almost all the later developed mapping functions, i.e., an elegant continuous fraction form representation:

$$m(\varepsilon) = \frac{1}{\sin\varepsilon + \frac{a}{\sin\varepsilon + \frac{b}{\sin\varepsilon + \frac{c}{\sin\varepsilon + \cdots}}}} \tag{2.19}$$

where the coefficients $a,b,c\ldots$ could be determined by surface meteorological parameters.

Niell Mapping Function

The Niell Mapping Function (NMF) is the most widely popular one for its high accuracy and conveniency. It does not rely on the surface meteorological parameters. The NMF specifies the three coefficients form of Marini mapping function (Niell, 1996):

$$m(\varepsilon) = \frac{1 + \frac{a}{1 + \frac{b}{1+c}}}{\sin\varepsilon + \frac{a}{\sin\varepsilon + \frac{b}{\sin\varepsilon + c}}} + \Delta H \tag{2.20a}$$

where the ΔH is the height correction term follows:

$$\Delta H = \left(\frac{1}{\sin\varepsilon} - \frac{1+\frac{a_{ht}}{1+\frac{b_{ht}}{1+c_{ht}}}}{\sin\varepsilon+\frac{a_{ht}}{\sin\varepsilon+\frac{b_{ht}}{\sin\varepsilon+c_{ht}}}}\right)\cdot\frac{H}{1000} \tag{2.20b}$$

And the a_{ht}, b_{ht}, c_{ht} are dimensionless constants, and H is scaled to km.

The highlights of this function lies on the determination of coefficients. The coefficients are different for hydrostatic and wet mapping functions. For the hydrostatic function, it takes account of both latitude dependency and the temporal variation of the coefficients. Accordingly, the hydrostatic coefficients x_H ($x = a, b, c$) of mapping function is modeled as a sinusoid function with period of one year at specific latitude φ:

$$x_H(\varphi, t) = x_{H,avg}(\varphi) + x_{H,amp}(\varphi)\, cos(2\pi\frac{t-T_0}{365.25}) \tag{2.21}$$

where $x_{\mathrm{H}}(\varphi, t)$ is the coefficient with average $x_{H,avg}(\varphi)$ and amplitude $x_{H,amp}(\varphi)$ which could be interpolated from a given lookup table of five distinct latitude bands. And t is the day of year (DOY) while T_0 is the phase, 28 or 211 for north or south hemisphere respectively. As for the wet mapping function, only the latitude dependency would be considered due to its high variability. The values of hydrostatic and wet coefficients could be calculated by a given lookup table and will not be listed here.

Vienna Mapping Function

The Vienna Mapping Function (VMF) has the same form as NMF while its coefficients are derived based on Numerical Weather Model (NWM), i.e., European Centre for Medium-Range Weather Forecasts (ECMWF). It has two versions, the rigorous and fast ones (Boehm & Schuh, 2004).In the rigorous version, all the coefficients, both hydrostatic and wet part, are estimated in a least squares procedure by ray tracing technique at ten different elevation angles. This version is very time consuming and only used for validation purpose.

For practical applications, a fast version VMF is developed in which only the coefficients a_{H} and a_{W} are estimated by ray tracing only at elevation angle of 3.3 ° and all the other coefficients are taken empirically from other mapping functions. And this fast version VMF is ten times faster than the rigorous version but

validated to reach the same accuracy. The fast VMF are released on a global grid (2.0°×2.5° latitude-longitude) every six hours. It has been proven to provide highest possible accuracy and been widely applied in geodetic and geophysical applications.

Global Mapping Function

The Global Mapping Function (GMF) could be seen as a backup of VMF which relies on external data source (Boehm et al., 2006). When VMF is not available, it can provide empirical values consistent with VMF. Actually, the GMF coefficients are derived from VMF and represented in spherical harmonics on a global grid:

$$x(\varphi,\lambda,t) = x_{avg}(\varphi,\lambda) + x_{amp}(\varphi,\lambda)\, cos(2\pi \frac{t-T_0}{365.25}) \quad (2.22)$$

$$x_i(\varphi,\lambda) = \sum_{n=0}^{9}\sum_{m=0}^{n} P_{nm}\,(sin\,\varphi)\cdot(A_{nm}\,cos\,m\lambda + B_{nm}\,sin\,m\lambda) \quad (2.23)$$

where $x(\varphi,\lambda,t)$ could be the hydrostatic or wet coefficients dependent on latitude, longitude and day of year (DOY) in a sinusoid form. And the mean value $x_{avg}(\varphi,\lambda)$ and amplitude $x_{amp}(\varphi,\lambda)$ are both expanded in nine order spherical harmonics with the subscript i denoting average or amplitude. The GMF could serve as a compatible empirical representation of VMF, making a good balance of accuracy and practicality.

2.3 Network RTK

Network RTK is an evolution of classical single baseline RTK technique. It can achieve centimeter level solution as single baseline RTK while largely extend the coverage. The Network RTK system is a comprehensive project involved with GNSS technology, computer technology and communication technology, and has been seen as civil infrastructure throughout the world.

2.3.1 Overview

Over decades, many reference station systems, or termed as Continuously Operating Reference Station (CORS), have been deployed all over the world for high accuracy applications, such as precise satellite orbits and clock generation, crustal deformation monitoring and earth rotation study. The basic conception of Network RTK technique is to takes advantage of these strategically distributed reference stations to

model the spatially correlated errors, like orbit error, tropospheric error and ionospheric error. In this way, the spatial decorrelation effect over distance could be overcome; thereby much larger area could be covered with only a few reference stations. The principle of Network RTK could be depicted in Figure 2.4 (SmartNet, 2016).

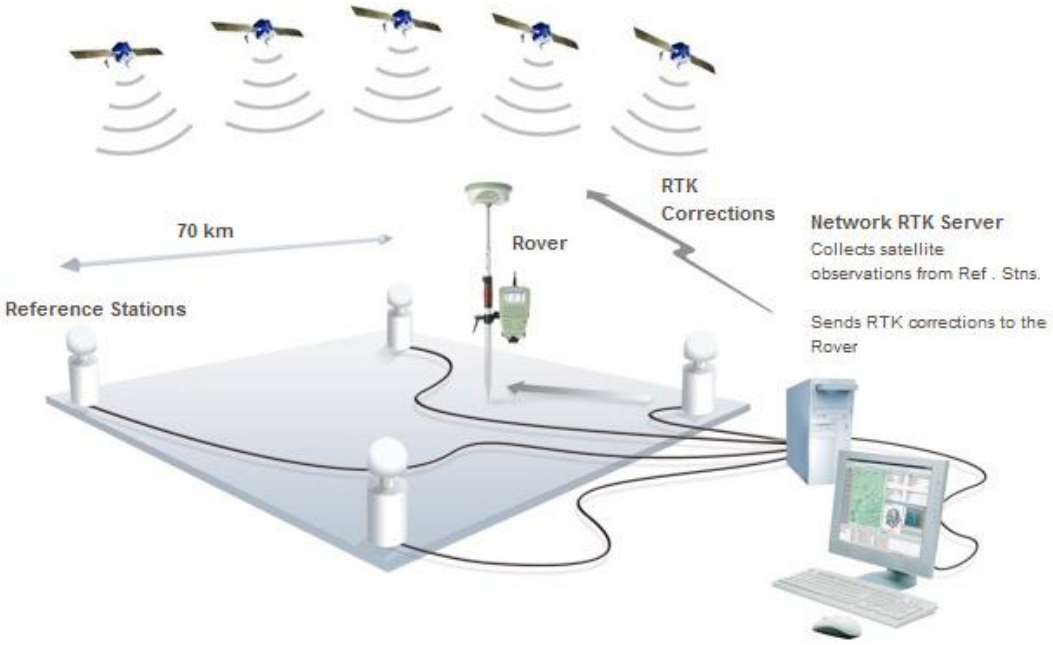

Figure 2.4 Principle of Network RTK

In the figure, the Network RTK technique is mainly composed of three main processes: network correction generation, correction interpolation and correction transmission (Lachapelle & Alves, 2002). Network correction generation mainly involves ambiguity resolution since the main observation is the carrier phase. To use the phase observation it is necessary to resolve the ambiguities. Once the ambiguities are correctly resolved, it is quite simple to derive various errors. After that, a proper model needs to be build to represent the relationship between the spatial position and the errors. The model is used to interpolate the errors at any position within the bounds of network and is crucial to the performance of Network RTK system. At last, the interpolated errors would be transmitted to the rover through Very High Frequency (VHF) or Ultra High Frequency (UHF) radio data link in specific protocols. It is notable that there are three popular concept of Network RTK technique, namely Virtual Reference Station (VRS), Flächenkorrekturparameter (FKP) and Master Auxiliary Concept (MAC), which are more related to the implementation of correction

transmission part. In this thesis, the focus is the error interpolation model, more specifically, tropospheric error.

2.3.2 Error Interpolation Models

A number of error interpolation models have been developed to predict spatial errors at the rover position in order to mitigate various error effects that degrade the carrier phase and pseudorange observations. The mathematical models of most commonly used interpolation models are introduced in this section.

Linear Interpolation Model

The Linear Interpolation Model (LIM) was first proposed by Wanninger (1995) to derive the regional ionospheric model. Actually, as a general function, this model could be applied for any type of error: later LIM was used to interpolate all the spatially correlated errors together (the combined error) without distinguishing (Rizos et al, 1999). The general model could be as follows:

$$\begin{bmatrix} v_1 \\ v_2 \\ \vdots \\ v_n \end{bmatrix} = \begin{bmatrix} X_1 & Y_1 \\ X_2 & Y_2 \\ \vdots & \vdots \\ X_n & Y_n \end{bmatrix} \cdot \begin{bmatrix} a \\ b \end{bmatrix} \tag{2.24}$$

where subscript n denotes different reference stations, v is the generated spatial error in the reference station, X, Y are the coordinates of reference station, and a, b are the model coefficients which could be estimated by a least squares adjustment:

$$\begin{bmatrix} \hat{a} \\ \hat{b} \end{bmatrix} = (A^T A)^{-1} A^T V \tag{2.25}$$

with

$$A = \begin{bmatrix} X_1 & Y_1 \\ X_2 & Y_2 \\ \vdots & \vdots \\ X_n & Y_n \end{bmatrix} \text{ and } V = \begin{bmatrix} v_1 \\ v_2 \\ \vdots \\ v_n \end{bmatrix} \tag{2.26}$$

And the error at the rover position v_u could be interpolated:

$$v_u = \hat{a} \cdot X_u + \hat{b} \cdot Y_u \tag{2.27}$$

Linear Combination Model

The Linear Combination Model (LCM) was proposed by Han and Rizos (1996). It is mainly designed to eliminate the orbit error while could also be effective to mitigate other spatial errors. The error for rover v_u

could be interpolated by:

$$v_u = \hat{a}_1 v_1 + \hat{a}_1 v_1 + \cdots + \hat{a}_n v_n \tag{2.28}$$

And the coefficients of LCM a_i should fulfill following conditions:

$$\begin{cases} \sum_{i=1}^{n} a_i = 1 \\ \sum_{i=1}^{n} a_i \left(\vec{X}_u - \vec{X}_i\right) = 0 \\ \sum_{i=1}^{n} a_i^2 = min \end{cases} \tag{2.29}$$

Distance Based Linear Interpolation Model

The Distance Based Linear Interpolation Model (DIM) was proposed by Gao et al (1997) and also originated for ionospheric error. It has the same form as LCM:

$$v_u = \hat{a}_1 v_1 + \hat{a}_1 v_1 + \cdots + \hat{a}_n v_n \tag{2.30}$$

But the coefficients are simple determined by the distance between the rover and reference station. It is based the assumption that the closer the rover locates to a reference station the more similar their atmospheric error should be. Hence, an inverse distance weight is taken to define the coefficients:

$$\hat{a}_1 = \frac{w_i}{w} \quad \text{with} \quad \mathrm{w_i} = \frac{1}{\mathrm{d_i}} \ , \ \mathrm{w} = \sum_{\mathrm{i=1}}^{\mathrm{n}} \mathrm{w_i} \tag{2.31}$$

where d_i is the distance of the rover to each reference station.

Lower Order Surface Model

The Lower Order Surface Model (LSM) is used to fit the spatial correlated errors to a regression surface. The low order usually refers to first or second order and the variables are usually the station horizontal coordinates. The height coordinate is always neglected in the case the error shows little correlation with height like the ionospheric error or there are small height difference among the reference stations. The typical models are given by Fotopoulos and Cannon (2001):

$$v = aX + bY + c \tag{2.32a}$$

$$v = aX + bY + cXY + d \tag{2.32b}$$

$$v = aX + bY + cXY + dX^2 + e \tag{2.32c}$$

$$v = aX + bY + cXY + dX^2 + eY^2 + f \tag{2.32d}$$

The second-order terms do not necessarily improve the model because they might be too sensitive to the

stochastic noise, thus result in oscillations which degrade the accuracy of modeling instead. In this sense, the simplest model 2.32a would give more robust and reliable results.

Chapter 3 Methodology

This chapter gives a detailed description of the approach applied in the thesis. Firstly, the general workflow is stated, followed by the procedures for the estimation of the ZTD, which makes the foundation for the subsequent investigation. Second, the Least Squares Collocation (LSC) method is introduced for modeling the regional tropospheric error. At last, a novel horizontal-altitude decomposition strategy is proposed to the model interpolation.

3.1 General Workflow

The major problem within this thesis is to investigate the tropospheric error interpolation models for the reference network with large height differences thus improving the accuracy of RTK solutions. The workflow is showed in Figure 3.1: the first stage is to derive the tropospheric error in the reference stations from continuous observations; and second is to build proper error interpolation models; finally the interpolated tropospheric error would be incorporated into the rover observations and accordingly the performance of interpolation models could be evaluated.

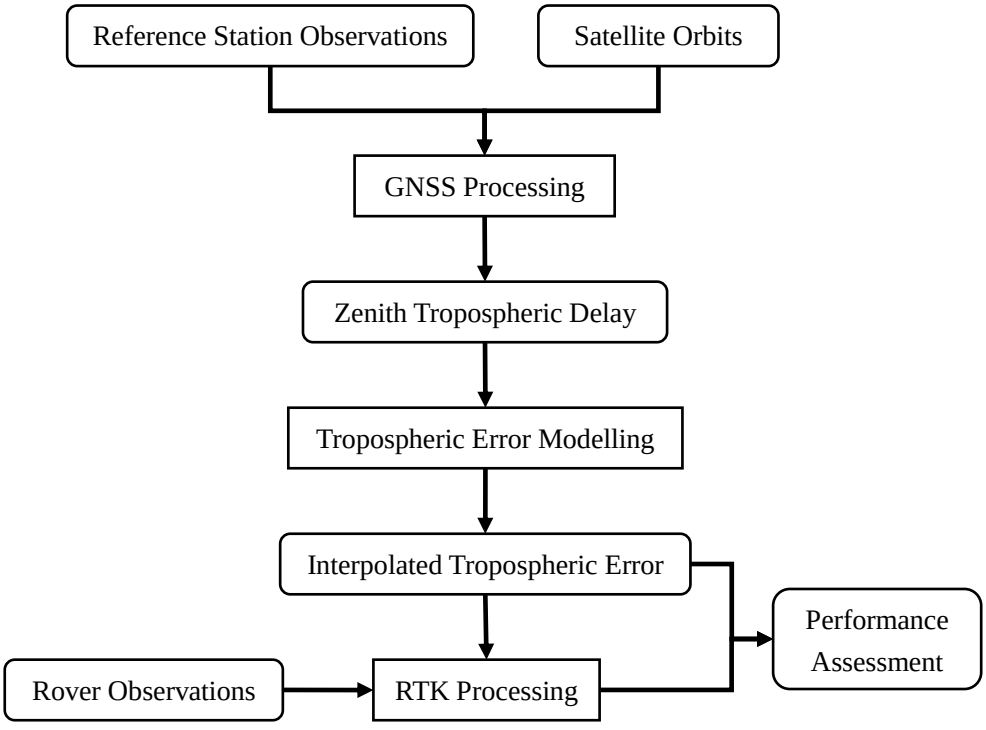

Figure 3.1 General workflow

3.2 ZTD Estimation from Bernese

GNSS processing has been proven to be of high accuracy for tropospheric delay estimation. In this thesis, the GNSS data was processed by the Bernese GNSS software (version 5.2) in order to obtain the ZTD. The Bernese GNSS software is developed by Astronomical Institute of the University of Bern (AIUB). It is a high performance, high accuracy and highly flexible reference GPS/GLONASS post-processing package and widely used in scientific research and high accuracy geodetic applications. Before the processing, the following files should be prepared, and listed in Table 3.1.

Table 3.1 Data preparation for GNSS processing

Filename Extension	File Directory	Descriptions
.PRE	/ORB	Satellite orbits
.IEP	/ORB	Pole information
.DCB	/ORB	Code differential bias
.*xx*O	/RAW	Raw RINEX observations, *xx* denoting two-digit years
.ION	/ATM	Ionosphere information
.GRD	/GRD	VMF coefficients for troposphere estimation
.ATL	/STA	Atmospheric tidal loading
.BLQ	/STA	Ocean tidal loading
.PLD	/STA	Tectonic plate assignment
.CRD	/STA	A priori reference coordinates
.ABB	/STA	Station name abbreviation
.CLU	/STA	Station cluster definition
.STA	/STA	Station information (receiver, antenna and problems)

After complementation of data preparation, the double-difference processing mode would be applied for a network solution by using the ionosphere-free linear combination observations (L3 observations in Bernese). In Figure 3.2, the main procedures for ZTD estimation are illustrated.

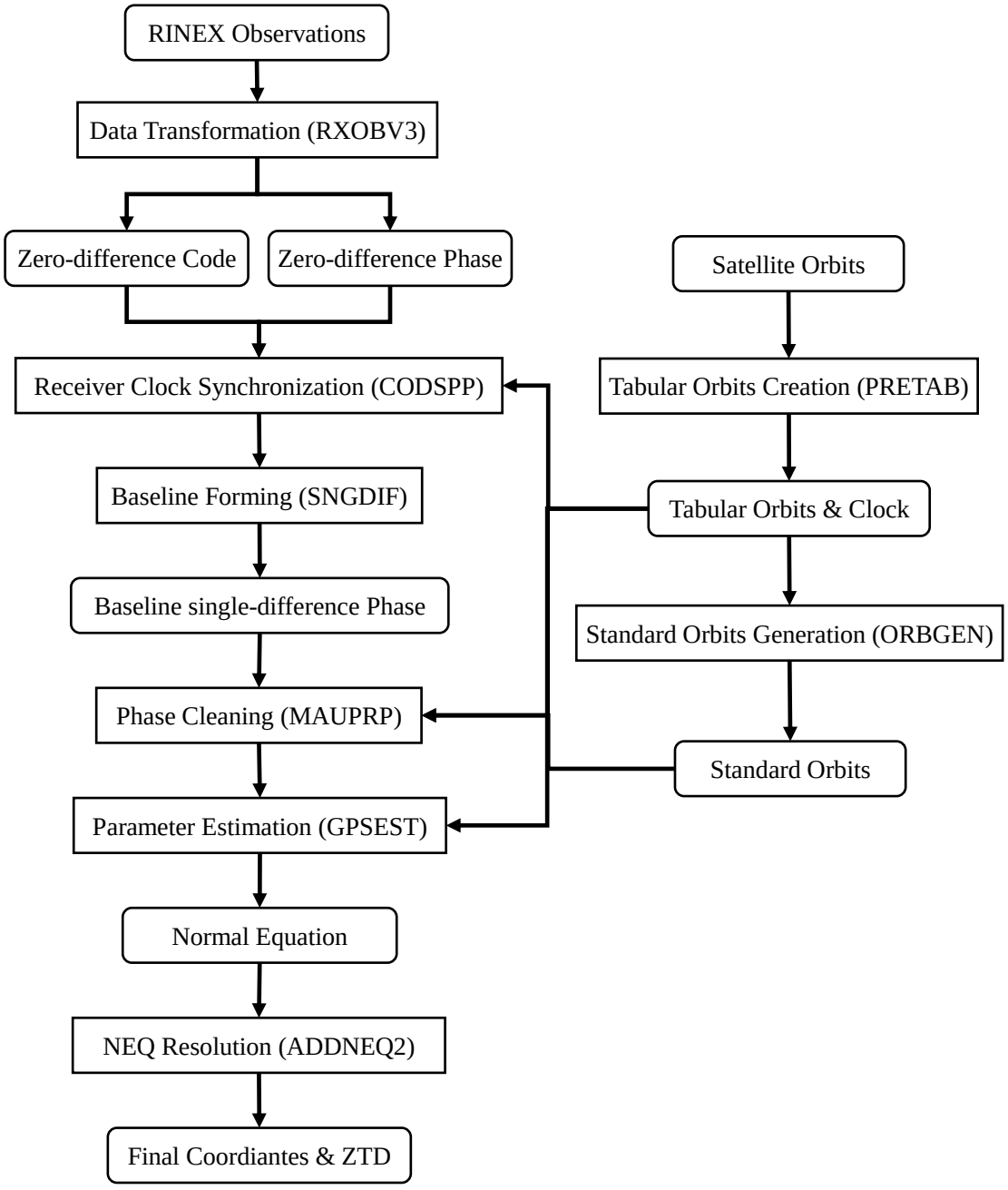

Figure 3.2 Main procedures for ZTD estimation

In the first step, the pole information would be extracted by program POLUPD. And then satellite orbits are generated with two programs PRETAB and ORBGEN. The PRETAB is used to create tabular orbits transforming from the terrestrial into the celestial reference frame and generate satellite clock. Subsequently the standard orbits in binary format are generated by ORBGEN, in which the tabular orbits

are taken as pseudo observations.

After generation of orbits, the GNSS data could be processed. First the RINEX raw observations are transformed to zero-difference code pseudorange and phase observation in Bernese format, which is conducted by RXOBV3. And then based only code observations, the receiver clock error are estimated with CODSPP. Then clock errors are saved in both code and phase observations and also used to reject outliers. Later, baseline single-difference observations are formed from the zero-difference observations by SNGDIF. The single-difference phase observations would be cleaned after the process of cycle-slip detection and repairing as well as outlier removal with MAUPRP. At last, the clean single-difference phase observations are used to form the double-difference phase observations which are the basis for parameter estimation by GPSEST. After solving the normal equations by ADDNEQ2, the station coordinates and ZTD could be obtained. Naturally, other parameters of interest could also be estimated with this general process.

The parameter estimation is conducted by GPSEST which is a least squares adjustment based program. It is an iterative process which mainly consists of four runs of GPSEST. In the first run, it is only aiming to generate the post-fit residuals for outlier rejection. So the L3 observations are resolved in real-valued ambiguities and many parameters are loosely set. After outliers screening, a first network solution would be generated in the second run. A preliminary estimation of ZTD results are produced also with float L3 ambiguities. Then in the third run, the ZTD would not be taken as unknowns. Instead, the preliminary ZTD estimation is incorporated for L3 ambiguity resolution baseline by baseline, and Quasi-Ionosphere-Free (QIF) strategy is used for most cases. At last run, the fixed integer ambiguities are introduced to the double-difference observation, and again the ZTD is taken into the estimation process. After the four rounds processing, the station coordinates and ZTD could be finalized.

3.3 A Least Squares Collocation Based Model

After GNSS data processing, the ZTD at each reference station could be obtained. The subsequent work is how to use these known spatially distributed observations to predict the ZTD at any other location. The problem is in essence a spatial data interpolation problem which is a general topic in Earth science

disciplines. In this thesis, the least squares collocation (LSC) method is introduced for the ZTD interpolation.

3.3.1 Least Squares Collocation

The LSC method was first proposed by Moritz (1972) to interpolate gravity anomaly and now is ubiquitous in the field of geodesy. In GNSS meteorology, it was implemented in the software package COMEDIE (COllocation of MEteorological Data for Interpolation and Estimation of tropospheric path delays) which is used to model the refractivity field using meteorological data (Troller et al., 2002). The LSC takes its name since it combines adjustment, filtering and prediction (Moritz, 1972).

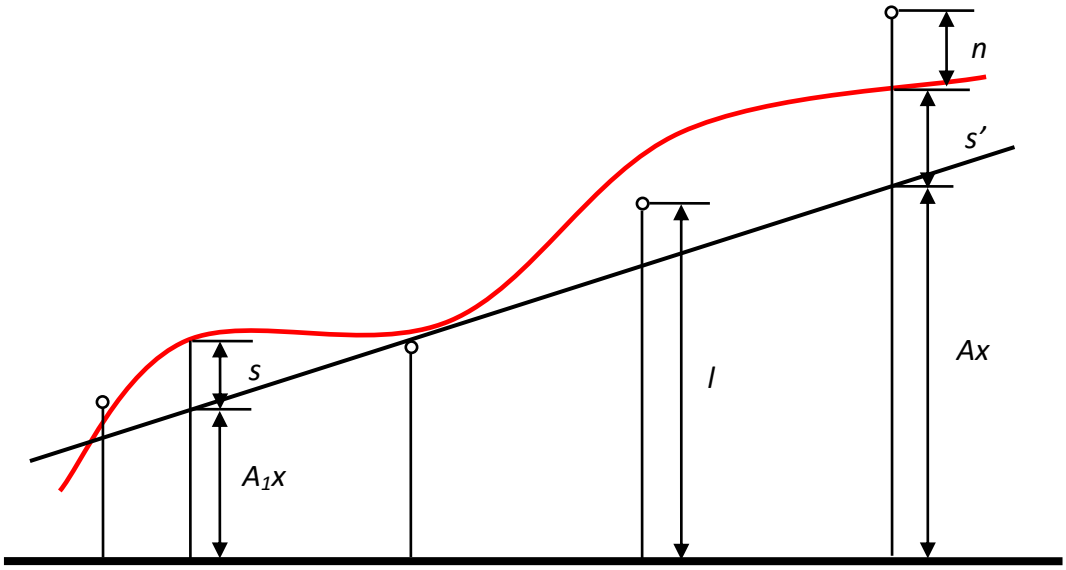

Figure 3.3 Principle of least squares collocation (Hurter, 2014)

In the classical least squares method, the observations are represented as a deterministic model suffered by white Gaussian noise, i.e., the estimated parameters are all nonrandom variable:

$$l = Ax + n \tag{3.1}$$

Instead, the LSC method takes into account the stochastic characteristics of observations in addition to the deterministic part. The basic model of LSC methods is expressed as follows:

$$l = Ax + s' + n \tag{3.2}$$

In figure 3.3, the principle of LSC method is briefly illustrated (Hurter, 2014). The red curve represents the truth, and the circles are measurements l. And the measurements contain three parts: (1) the deterministic part or the trend part Ax, where A is the design matrix and x the unknown parameters, represented by the slant line; (2) the stochastic part or signal s'; (3) the white Gaussian noise n. As for the interpolation point, the noise is filtered thus it contains just deterministic part plus the signal.

The underlying rationale is that the truth cannot be fully represented by a deterministic model and remaining part shows non-Gaussian stochastic property. So it is sensible to add a so-called signal part to make up the deterministic model. The parameters include both random and nonrandom variables. In the following, a brief derivation of the LSC will be given for better understanding.

Let s' to be the signal corresponding to the measured points and s the signal corresponding to the interpolation points. The stochastic model of them follows:

$$E(s') = 0, \quad C_{s's'} = E(s's'^T) \tag{3.3a}$$

$$E(s) = 0, \quad C_{ss} = E(ss^T) \tag{3.3b}$$

And let $\Lambda = [s \;\; s']$ and $B = [I \;\; O]^T$, thus the LSC model including both measured points and interpolation points could be given:

$$l = Ax + B\Lambda + n \tag{3.4}$$

with

$$C_{\Lambda\Lambda} = \begin{bmatrix} C_{s's'} & C_{s's} \\ C_{ss'} & C_{ss} \end{bmatrix} \tag{3.5a}$$

$$C_{ll} = BC_{\Lambda\Lambda}B^T + C_{nn} \tag{3.5b}$$

$$P_n = {C_{nn}}^{-1} \tag{3.6a}$$

$$P_\Lambda = {C_{\Lambda\Lambda}}^{-1} \tag{3.6b}$$

$$P_l = {C_{ll}}^{-1} \tag{3.6c}$$

The error equation reads:

$$v = A\hat{x} + B\hat{\Lambda} - l \tag{3.7}$$

In a least square sense, the objective function should be minimum:

$$\Omega = v^T P_n v + \hat{\Lambda}^T P_\Lambda \hat{\Lambda} \tag{3.8}$$

By forming:

$$\frac{\partial \Omega}{\partial \hat{x}} = 2v^T P_n A = 0 \tag{3.9a}$$

$$\frac{\partial \Omega}{\partial \hat{\Lambda}} = 2v^T P_n B + 2\hat{\Lambda}^T P_\Lambda = 0 \tag{3.9b}$$

The resolution could be obtained:

$$\hat{x} = (A^T P_l A)^{-1} A^T P_l l \tag{3.10a}$$

$$\hat{\Lambda} = {P_\Lambda}^{-1} B^T P_l (l - A\hat{x}) \tag{3.10b}$$

And $\widehat{\Lambda}$ could be decomposed:

$$\hat{s}' = C_{s's'} {C_{ll}}^{-1} (l - A\hat{x}) \tag{3.11a}$$

$$\hat{s} = C_{ss'} {C_{ll}}^{-1} (l - A\hat{x}) \tag{3.11b}$$

The value of interpolated points:

$$l_p = A\hat{x} + \hat{s} \tag{3.12}$$

3.3.2 Deterministic Model

The zenith tropospheric delay (ZTD) is composed of the zenith hydrostatic delay (ZHD) and the zenith wet delay (ZWD). The ZHD could be estimated by an empirical model with high accuracy. Therefore, only the ZWD will be interpolated and two deterministic models would be investigated. The first is a low order surface model with consideration of the height factor:

$$ZWD = aX + bY + cH + d \tag{3.13a}$$

The second deterministic model is based on physical realities (Troller, 2004). The correlation between ZWD and height could be described by negative exponential function:

$$ZWD = (aX + bY + d) \cdot e^{-H/c} \tag{3.13b}$$

where a, b are coefficients for horizontal gradients, c is for the correlation with height and d is constant trend for the ZWD.

3.3.3 Covariance Function

The covariance function describes the spatial behavior of measurements. It is an important topic in the framework of spatial analysis. In the spatial domain, the covariance function is naturally a function of

spatial distance and it has to fulfill the following requirements: (1) it should be positive definite; (2) it decays with distance increasing; (3) it is symmetric with respect to distance. In Table 3.2, some common covariance functions used in the geodetic fields are listed (Darbeheshti, 2009).

The Gaussian covariance function is suited to represent a smoothly varying spatial process and is applied in this work. However, the correlation length d and scaling factor C_0 are usually empirically determined. And there is a high possibility that they are varying with different places due to the differences of physical conditions.

Table 3.2 Common Covariance Functions

Name	Function	Special Parameter
Exponential	$C_0 e^{-\frac{rln2}{d}}$	
Gaussian	$C_0 e^{-\frac{r^2}{d^2}}$	
Triangular	$C_0(1-\frac{r}{\alpha d})$	$\alpha = 2$
Second-order Markov	$C_0(1+\frac{r}{\alpha d})e^{-\frac{r}{\alpha d}}$	$\alpha \approx 0.52$
Third-order Markov	$C_0(1+\frac{r}{\alpha}-\frac{r^2}{2\alpha^2})e^{-\frac{r}{\alpha}}$	$d = 1.095\alpha$
Spherical	$C_0(1-0.5\frac{r}{\alpha d}-0.5\left(\frac{r}{\alpha d}\right)^3)$	$\alpha \approx 2.87939$

In this work, the parameters of covariance function are determined iteratively: (1) the least squares adjustment is used to initialize the residuals; (2) the residuals are used to fit an initial covariance function; (3) the estimated covariance function is incorporated into the least squares collocation (LSC) procedure for derivation of parameter and residuals; (4) repeat step 2 and 3 until convergence.

After removing the deterministic part or the trend part, the remaining residuals are in millimeter level. And the estimation converges after two iterations. In figure 3.4, the blue line shows a fitted the Gaussian covariance function, and the red scatters denote the covariance from the observation data. The fitted covariance function decays to zeros with increasing distance between two receivers.

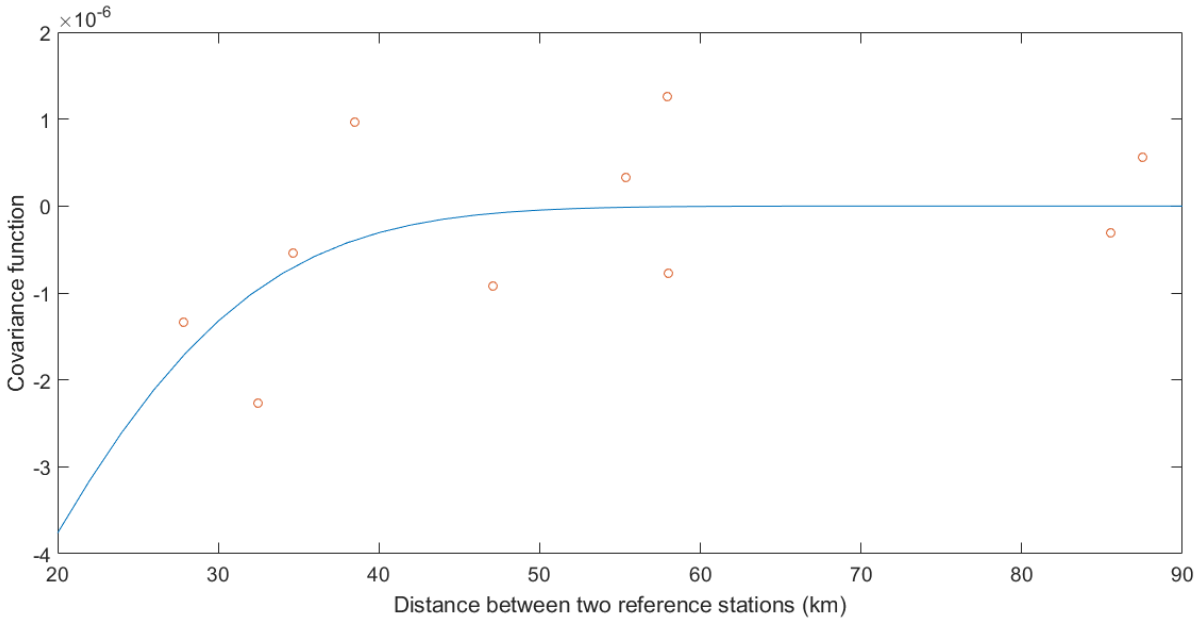

Figure 3.4 Fitted covariance function with respect to station distance

3.4 Horizontal-height Decomposition Model

The zenith wet delay (ZWD) is influenced by the horizontal position and height of the station. The spatial behavior of ZWD is different in the horizontal and height direction. In the horizontal, it shows linear trend unless the cases of extreme weather. While in the height direction, it decreases with increasing height in a negative exponential way (Troller, 2004). In this sense, it is advisable to decompose the ZWD into two parts:

$$ZWD(X,Y,H) = ZWD(X,Y) + ZWD(H) \tag{3.14}$$

where $ZWD(X,Y)$ is the horizontal correlated part, and $ZWD(H)$ the height correlated part.

Then the question lies on how to make the decomposition for the estimated ZWD. Here an empirical ZWD model should be introduced to determine the global scaling factor β:

$$ZWD(X,Y,H) = \beta \cdot ZWD_0(X,Y,H) \tag{3.15}$$

where $ZWD(X,Y,H)$ is the estimated ZWD at the reference station , and $ZWD_0(X,Y,H)$ is the empirical value from a model, and they are connected by the scaling factor β. The empirical model could be chosen as either Saastamoinen or Hopfield model, since their values are quite close in the same condition.

Now the empirical ZWD could be decomposed. First, the horizontal correlated part is derived:

$$ZWD_0(X,Y) = ZWD_0(X,Y,H_0) \tag{3.16a}$$

where $ZWD_0(X,Y,H)$ is the empirical ZWD at station height H, and $ZWD_0(X,Y,H_0)$ is the empirical ZWD at a reference height H_0, and H_0 could be set as the mean height of all the reference stations. Accordingly, the height correlated ZWD is the remaining part:

$$ZWD_0(H) = ZWD_0(X,Y,H) - ZWD_0(X,Y) \tag{3.16b}$$

It is assumed that the empirical ZWD, both the horizontal or height correlated component suffer the same dilation or shrinkage, which is defined by the scaling factor β. Thus, the estimated ZWD is decomposed as follows:

$$ZWD(X,Y) = \beta \cdot ZWD_0(X,Y) \tag{3.17a}$$

$$ZWD(H) = \beta \cdot ZWD_0(H) \tag{3.17b}$$

After the decomposition, the horizontal part and height part could be processed by different interpolation models, e.g. the horizontal part simply by distance based linear interpolation model (DIM), and the height part by the negative exponential model. After that they are combined to form the total interpolated ZWD.

$$ZWD(X,Y,H) = ZWD(X,Y) + ZWD(H) \tag{3.18}$$

Chapter 4 Experiments and Analysis

In this chapter, details of the experiments and corresponding results are presented, according the approach described in Chapter 3. At first, an overall description of experimental scenario is given. Then, the impact of large height difference for the height component is introduced. After that, the focus is put the performance of different error interpolation models. Finally, the influence of network configuration is investigated, with respect to the number, baseline length and distribution of the reference stations.

4.1 Overall Description

The GNSS raw observations for experiment are provided by LDBV. The RINEX files with 1s sampling rate include 1day observations of 9 SAPOS reference stations and an additional reference station named KIT. Besides, two rover stations named Oberau and 8553 are set for just a few hours. All these stations locate in the Bavaria state, i.e., in the Garmisch-Patenkirchen area. The SAPOS network is a CORS (Continuously Operating Reference Stations) network in Germany based on a nationwide network of more than 270 reference stations across Germany (SAPOS flyer, 2015). Station KIT is temporally set up by Institute of Meteorology and Climate Research-Atmospheric Environmental Research (IMK-IFU) of Karlsruhe Institue of Technology (KIT) for atmospheric research. The basic information of the stations involved in the following test is listed in Table 4.1 and 4.2.

Table 4.1 Basic information of SAPOS reference stations

Site Name	Latitude	Longitude	Height	Antenna type	Description
MUENCHEN	48.14108	11.59010	579.73733	TRM59800.00	Choke Ring
WERTACH	47.60227	10.41563	955.35465	TRM59800.00	Choke Ring
BAD TOELZ	47.76113	11.56785	741.70645	TRM55971.00	Choke Ring
ROSENHEIM	47.86756	12.10703	521.90181	TRM59800.00	Choke Ring
MINDELHEIM	48.04201	10.49406	671.87757	TRM59800.00	Choke Ring
GARMISCH	47.50926	11.14273	1827.87199	TRM59800.00	Choke Ring
LINDAU	47.55888	9.70806	473.33963	TRM59800.00	Choke Ring
WEILHEIM2	47.83816	11.14308	628.54553	TRM59800.00	Choke Ring

PATSCHERKOFEL	47.20800	11.46019	2298.31598	LEIAR25.R3	Choke Ring

Table 4.2 Basic information of KIT and rover stations

Site Name	Latitude	Longitude	Height	Antenna type	Description	Time span
KIT	47.47645	11.06316	794.10349	TRM29659.00	Choke Ring	
Oberau	47.55471	11.14293	702.12774	LEIAT504GG	Choke Ring	10:41:55 - 12:49:53
8533	47.48939	11.25237	953.78248	LEIAT504GG	Choke Ring	06:32:52 - 09:28:48

All the receivers are dual frequency high precision geodetic grade equipped with the Choke Ring antenna which effectively mitigate the multipath effects. In order to obtain the ground truth of ZTD and the coordinates of reference and rover stations, the one day raw RINEX observations are processed by the Bernese GNSS software. The SAPOS reference stations, the KIT station and two rover stations form a local network. In order to define a geodetic datum for the local network, six IGS tracking stations are introduced, namely MARS, NOT1, ONSA, SOFI, WROC and WSRT which locate around the local network with long distance. Another benefit of introducing the IGS stations is to decorrelate the ZTD estimation in a small network (Dach et al, 2007), thus the absolute ZTD could be obtained. In Table 4.3, the basic settings of Berness GNSS processing are summarized.

Table 4.3 Basic settings of Berness processing

	Descriptions
Processing mode	Static, double difference, ionosphere-free combination L3 observations
Cutoff angle	3°, $\cos z$ weighting
Orbit product	CODE final orbits
Sampling rate	30s
A priori troposphere	Dry VMF model
Estimated troposphere	Wet VMF model in 1 hour spacing
Ambiguity resolution	Quasi-ionosphere-free (QIF) strategy
Datum definition	Minimum constraint solution, no-net translation condition

CHAPTER 4 EXPERIMENTS AND ANALYSIS

After processing by Berness GNSS software, the static coordinates and ZTD of all the involved stations could be obtained. A posteriori RMS of unit weight is 0.00152 m. In Table 4.4, the RMS errors of station coordinates are listed.

Table 4.4 RMS error of station coordinates (m)

Site Name	X	Y	Z	U	N	E
MUENCHEN	0.00031	0.00014	0.00033	0.00044	0.00013	0.00011
WERTACH	0.00033	0.00014	0.00035	0.00047	0.00014	0.00012
BAD TOELZ	0.00032	0.00014	0.00034	0.00045	0.00013	0.00011
ROSENHEIM	0.00031	0.00013	0.00033	0.00043	0.00013	0.00011
MINDELHEIM	0.00031	0.00013	0.00033	0.00044	0.00013	0.00011
GARMISCH	0.00031	0.00013	0.00033	0.00044	0.00013	0.00011
LINDAU	0.00033	0.00014	0.00034	0.00046	0.00013	0.00012
WEILHEIM2	0.00031	0.00013	0.00032	0.00043	0.00013	0.00011
PATSCHERKOFEL	0.00033	0.00014	0.00035	0.00046	0.00014	0.00012
KIT	0.00043	0.00027	0.00048	0.00062	0.00017	0.00026
Oberau	0.00313	0.00319	0.00303	0.00424	0.00181	0.00281
8533	0.00141	0.00102	0.00128	0.00179	0.00062	0.00104

In Figure 4.1, the estimated ZTD of IGS station ONSA is compared with CODE troposphere products. The maximum difference is 1.3cm and most differences are within millimeter level. It shows the estimated ZTD has a good correspondence with the CODE product. Hence, it is demonstrated that reliable absolute ZTD of above mentioned stations has been obtained for ground truth. And in Figure 4.2 and 4.3, the height of 9 SAPOS reference stations and KIT station and corresponding daily mean ZTD are illustrated separately, and a clear negative correlation could be found.

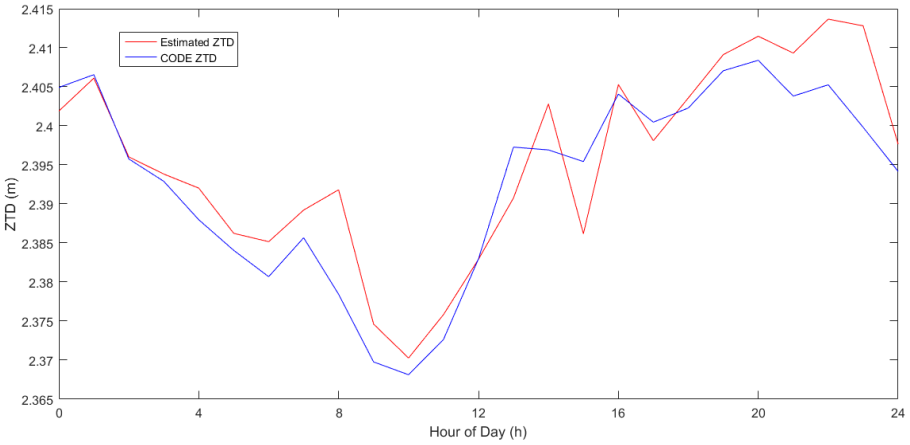

Figure 4.1 Estimated ZTD and CODE ZTD comparison in ONSA

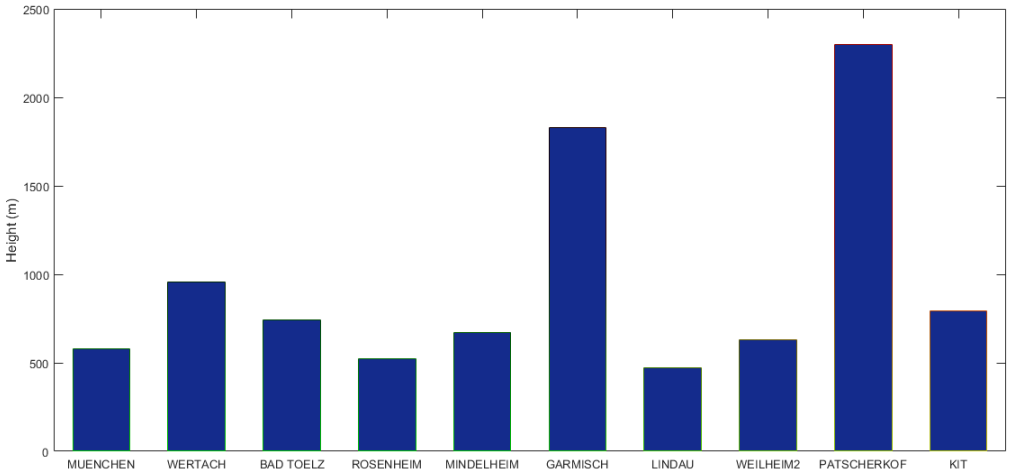

Figure 4.2 Height distributions of different stations

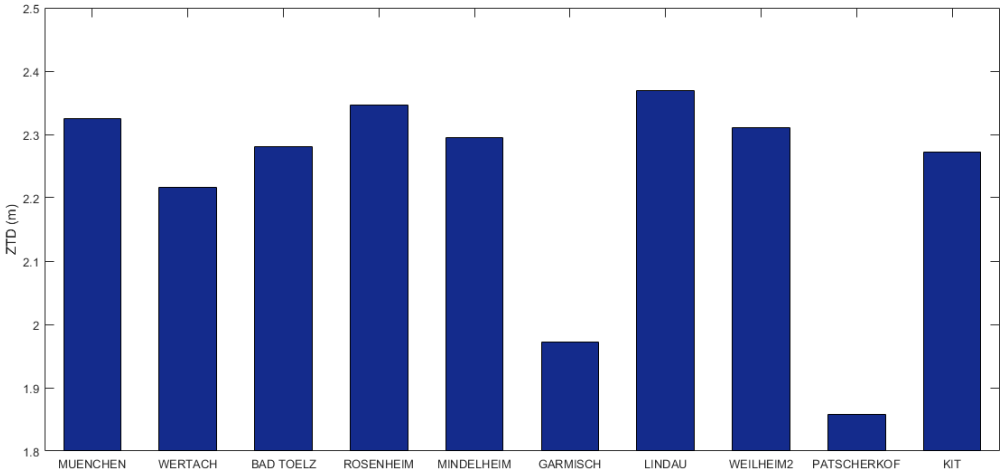

Figure 4.3 Daily mean ZTD of different stations

4.2 Positioning under Large Height Difference

In a first step, it is sensible to investigate the influence for positioning of height difference. For this purpose, two reference stations are chosen, namely GARMISCH and KIT. The baseline of the two stations is quite short at around 7km while the height difference between them is above 1000m, the mean difference of ZTD and ZWD is around 30cm and 4cm respectively, which makes suitable condition for investigation.

In this part, only the empirical models would be applied to correct the tropospheric delay error. This is to simulate the baseline processing of commercial GNSS processing softwares, i.e., Trimble Business Center, Leica Geo Office and GrafNav. In this case, the common ZTD is canceled in the differencing process, and the remaining part would be compensated with the help of the empirical model, thus largely reducing the tropospheirc effect. Two classic empirical models are introduced for investigation: Saastamoinen model and Hopfield model. The station GARMISCH is fixed as base station and KIT is taken as the rover. In Figure 4.4 and 4.5, the positioning errors in horizontal and height direction of station KIT are illustrated respectively.

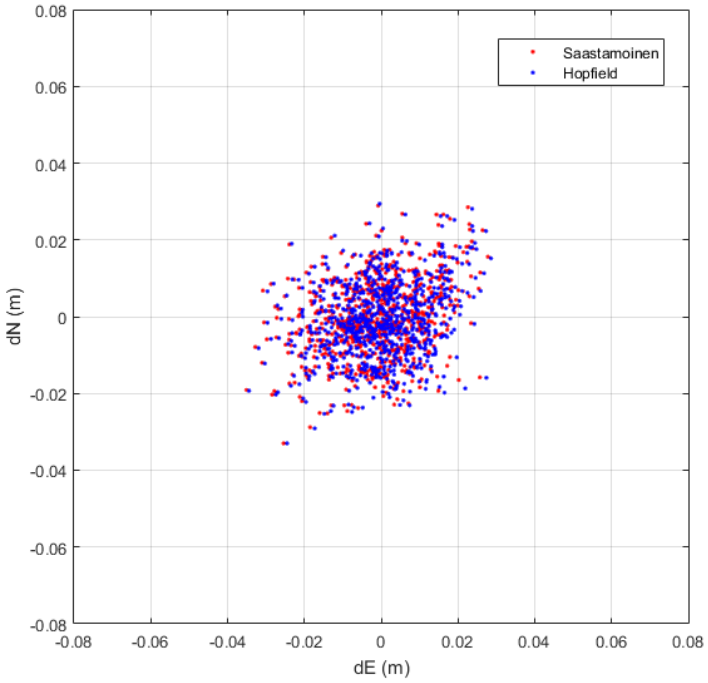

Figure 4.4 Horizontal errors of KIT

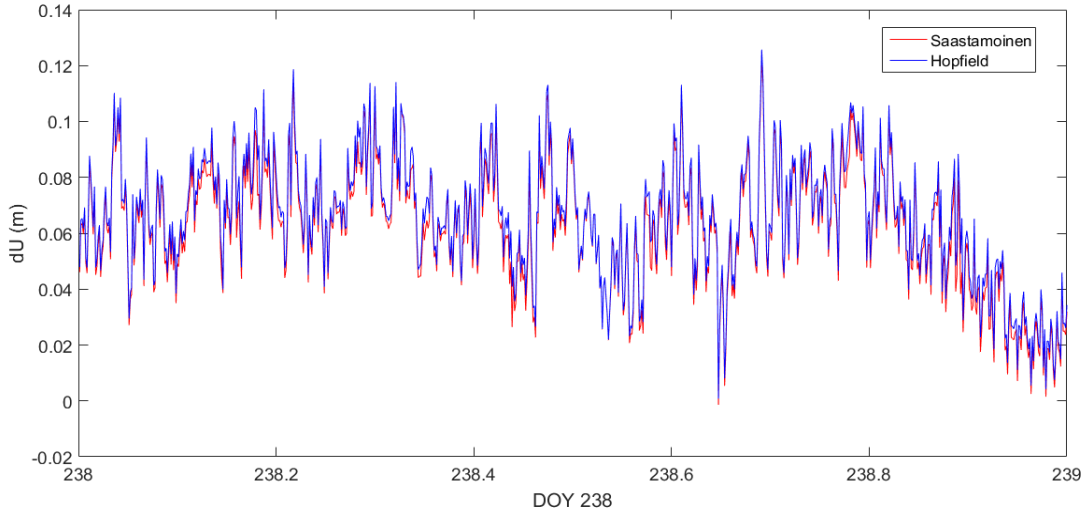

Figure 4.5 Height errors of KIT

Figure 4.4 shows that the positioning errors for the horizontal component fall within ±4 cm in the east direction and ±3 cm in the north direction, and overwhelming majority (over 95%) are within ±2cm and evenly distributed in both the positive and negative part. However, in Figure 4.5 there exists systematic bias for the height component since all the errors are in the positive side. Besides, the height errors exhibit large variation over time and the maximum reaches up to 13cm. In Table 4.5, the main statistics of height error are listed. It can be concluded that the remaining uncorrected tropospheric error mainly degrades the height positioning accuracy. Both the Saastamoinen model and Hopfield model have the same level of performance and empirical models have limited capability to mitigate the tropospheric error. In the following part, the interpolation models of the tropospheric error will be emphasized, especially on the improvement for the height component.

Table 4.5 Main statistics of height error by empirical models (m)

	Saastamoinen Model	Hopfield Model
MAX	0.1231	0.1257
MIN	-0.0014	0.0008
AVG	0.0624	0.0658
STD	0.0214	0.0215
RMS	0.0660	0.0692

4.3 Performance Comparison with Different Models

In this section, the tropospheric delay at the rover position will be interpolated with the nearby reference stations. And the different interpolation models will be compared in two aspects: the first is the tropospheric delay interpolation error, and the second is the height component error in positioning. For this investigation, six reference stations are involved, namely, WERTACH, WEILHEIM2, BAD TOELZ, GARMISCH, PATSCHERKOFEL, and KIT. In Figure 4.6, the configuration of these stations is briefly illustrated, the upper one shows the horizontal layout of stations in which the triangles denote the four reference stations and the circle is KIT regarded as a rover station again, and the lower figure depicts the height difference of different reference station with respect to the rover station KIT.

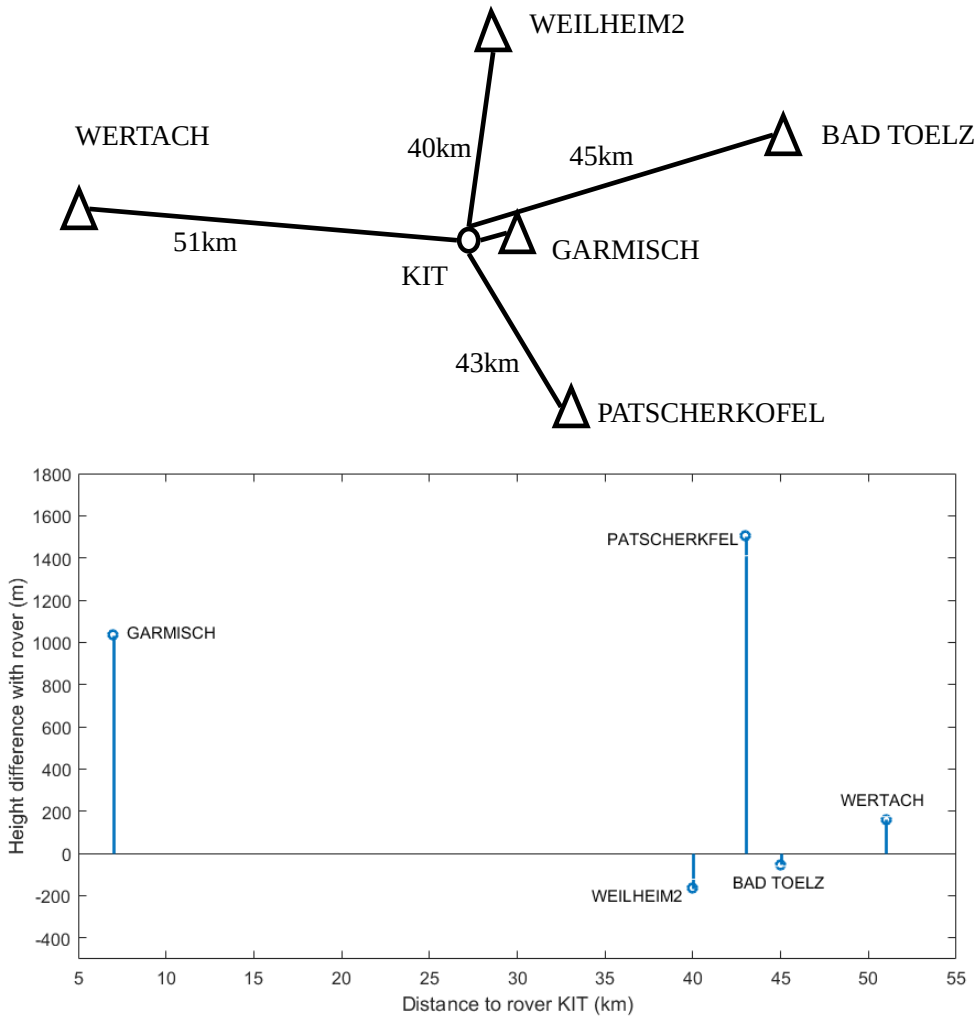

Figure 4.6 Network configuration 1

4.3.1 Accuracy of Troposphere Error Interpolation

At first, the accuracy of different troposphere interpolation model will be evaluated since it is critical for the performance of positioning. It is also the reason for taking KIT as a rover but not a real rover, since the ground truth could provide one day tropospheric delay in KIT station for comparison. In Figure 4.6, the interpolation models described above are compared: linear interpolation model (LIM), linear combination model (LCM), distance based linear interpolation model (DIM), the linear form least squares collocation model (LSC) and the horizontal-height decomposition model (HHD). The interpolated ZWD is subtracted by the truth, resulting in the interpolation error as shown in Figure 4.7.

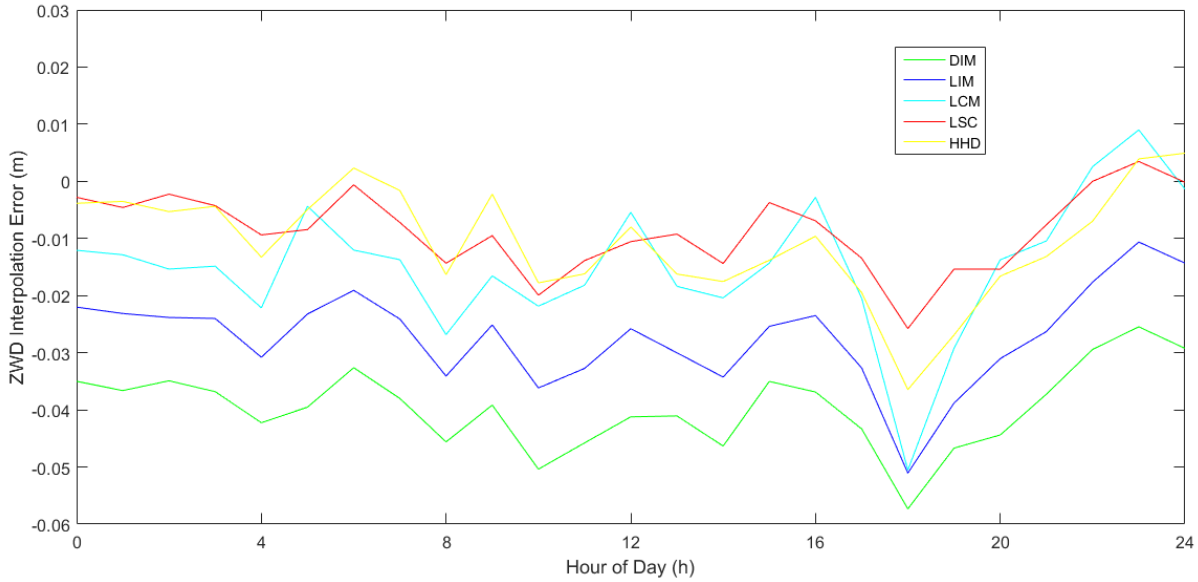

Figure 4.7 ZWD interpolation errors of different models

The DIM performs the worst for its distance based weighting strategy. The KIT is much closer to GARMISCH station compared to other reference stations. So the contribution of GARMISCH is much larger than others. However, the existing large height difference between KIT and GARMISCH will introduce large bias for the interpolation, as shown in Figure 4.7. The LIM, LCM, LSC and HHD has similar pattern due to their mathematical expression. The LIM takes no consideration of the height component, and the interpolated ZWD is only linearly determined by the horizontal coordinates. The LCM accounts for the 3D coordinates and it performs much better than the DIM and LIM. However its formula is originally derived in aim to eliminate the orbit error. As for troposphere modeling, it has no really physical meanings. In the LSC and HHD, the tropospheric delay is modeled as a function of station height, in linear

or exponential form. By this way, the systematic bias caused by height could be mitigated. As shown in Figure 4.7, the two models have compatible performance. For most interpolated ZWD, the errors are within ±1.5cm except the one at 18:00-19:00. The interpolation error reaches approximately -3cm, twice as large as the normal ones. It could be found that all the models show the same pattern during that time period. So a possible explanation could be that extreme weather happened at that time, which largely deteriorated the spatial correlation in the network area. In Table 4.6, the main statistics of ZWD interpolation errors of difference models are listed for better comparison. The LSC and HHD outperform the others with respect to the ZWD interpolation accuracy.

Table 4.6 Main statistics of ZWD error of different models (cm)

	LIM	DIM	LCM	LSC	HHD
MAX	-5.11	-5.73	-5.05	-2.58	-3.65
AVG	-2.72	-3.96	-1.47	-0.86	-1.05
RMS	2.84	4.02	1.86	1.10	1.42

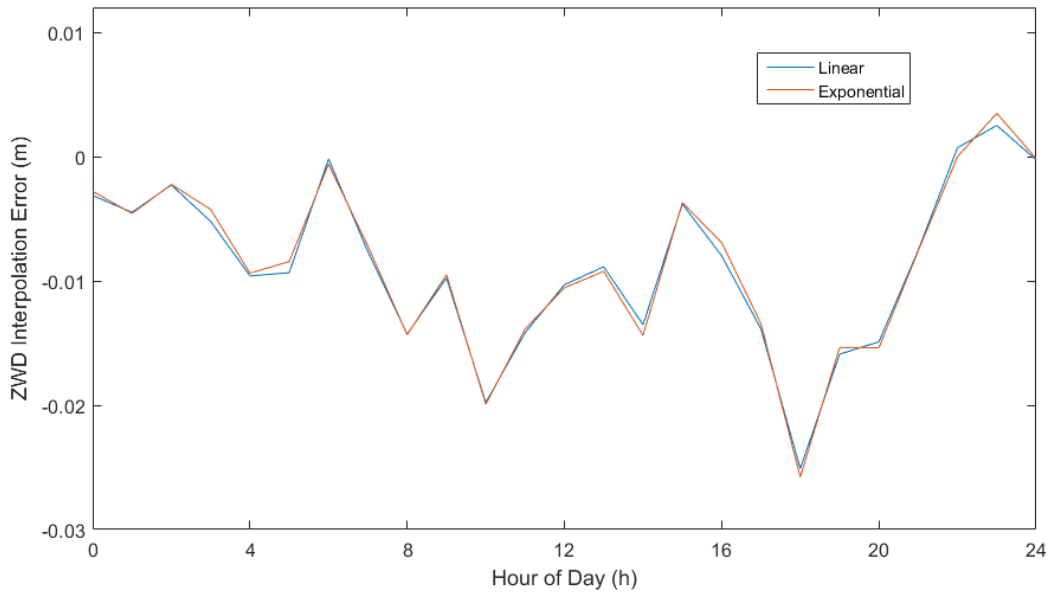

Figure 4.8 Comparison of linear and exponential LSC

In Figure 4.8, the linear and exponential form LSC are compared. It is concluded that there is no obvious difference with respect to their performance. The difference of them is in sub millimeter level which is negligible compared to the interpolation error. The reason is that the estimated exponent with respect to

height is quite small, in the order of 10^{-4}/km. So the exponential function could be approximated by a Taylor series neglecting all the terms of order higher than 1. Therefore, it is advisable to use a simple linear LSC for troposphere modeling which is able to achieve centimeter accuracy under normal weather.

4.3.2 Accuracy of RTK Positioning

With the interpolated tropospheric delay, the observations at the rover could be corrected to improve RTK positioning. In the following part, the performance of RTK positioning of above models will be evaluated. The height component errors of different models are illustrated in Figure 4.9.

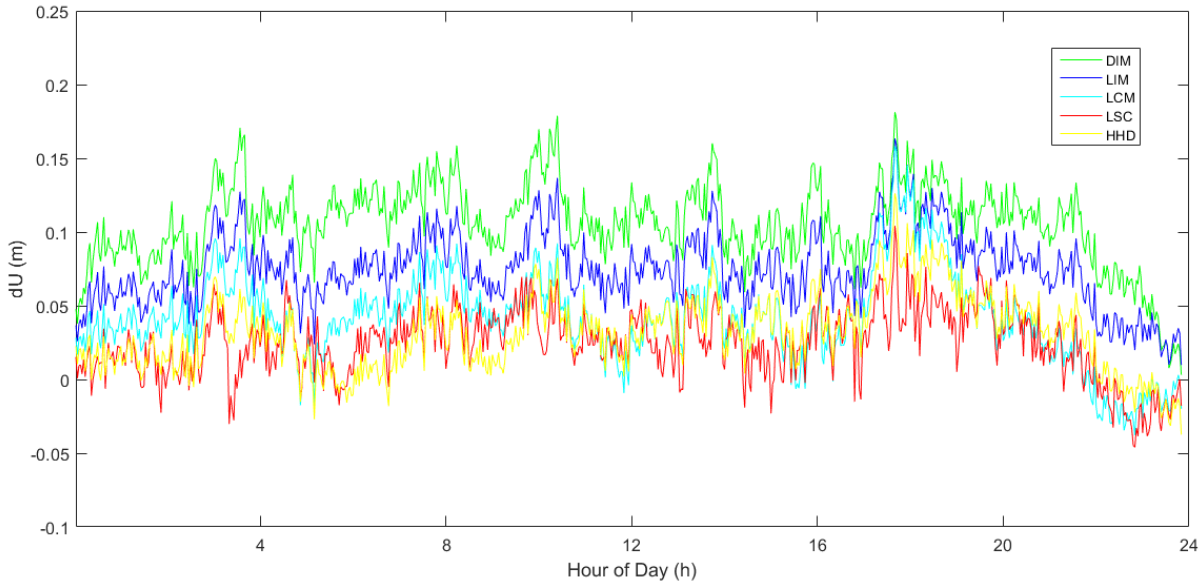

Figure 4.9 Height errors of different models

It is obvious that the height component error negatively correlates with the ZWD interpolation errors. And it follows an empirical rule that 1cm tropospheric delay would result in 3-4cm height error. The DIM and LIM both introduce large systematic bias without consideration of height. The height errors of DIM mostly exceed 10cm while errors of LIM locate within 6-10cm. During 18:00-19:00, the height error of different models jumps to maximum due to the large ZWD errors possibly caused by an extreme weather event. The height error statistics is listed in Table 4.7. Besides, it is better to form a cumulative distribution function (CDF) of the height errors for evaluation in Table 4.8. Therefore, it is concluded that with consideration of the correlation of height, better interpolated tropospheric delay could improve the performance of positioning. But for the case that extreme weather occurs, it is not able to work out. A possible solution is to

densify the reference network which will be discussed in the outlook.

Table 4.7 Main statistics of height error of different models (cm)

	LIM	DIM	LCM	LSC	HHD
MAX	18.13	16.35	15.83	10.42	12.62
AVG	10.59	7.48	4.14	2.43	3.12
RMS	10.95	7.86	5.17	3.36	4.02

Table 4.8 CDF of height error of different models (cm)

	< =2	<=4	<=6	<=10
DIM	0.97%	2.22%	5.28%	38.33%
LIM	0.83%	8.33%	24.31%	84.44%
LCM	19.03%	48.47%	77.92%	95.28%
LSC	39.86%	74.58%	94.03%	99.17%
HHD	34.03%	63.75%	87.50%	98.61%

4.4 Influence of Network Configuration

Network configuration assumes a critical role in the Network RTK system. The number of nearby reference stations for interpolation, the distance to nearby reference stations and the distribution of them are three factors that will be investigated in the following part. Two real rovers with short period observations (approximately 2 to 3 hours) are introduced locating in the valley of Garmisch-Patenkirchen area, whose marker names are Oberau and 8533.

4.4.1 Number of Reference Stations

The station KIT is temporally set for atmospheric research by Institute of Meteorology and Climate Research-Atmospheric Environmental Research (IMK-IFU) of Karlsruhe Institue of Technology (KIT). Unlike previous section, here it is taken as a reference station to investigate its effect for performance improvement. A small network is chosen and its configuration is shown in Figure 4.10, two circles denoting the rovers, and the lower two figures show the height difference of reference stations with respect to the

rover stations Oberau and 8533 respectively.

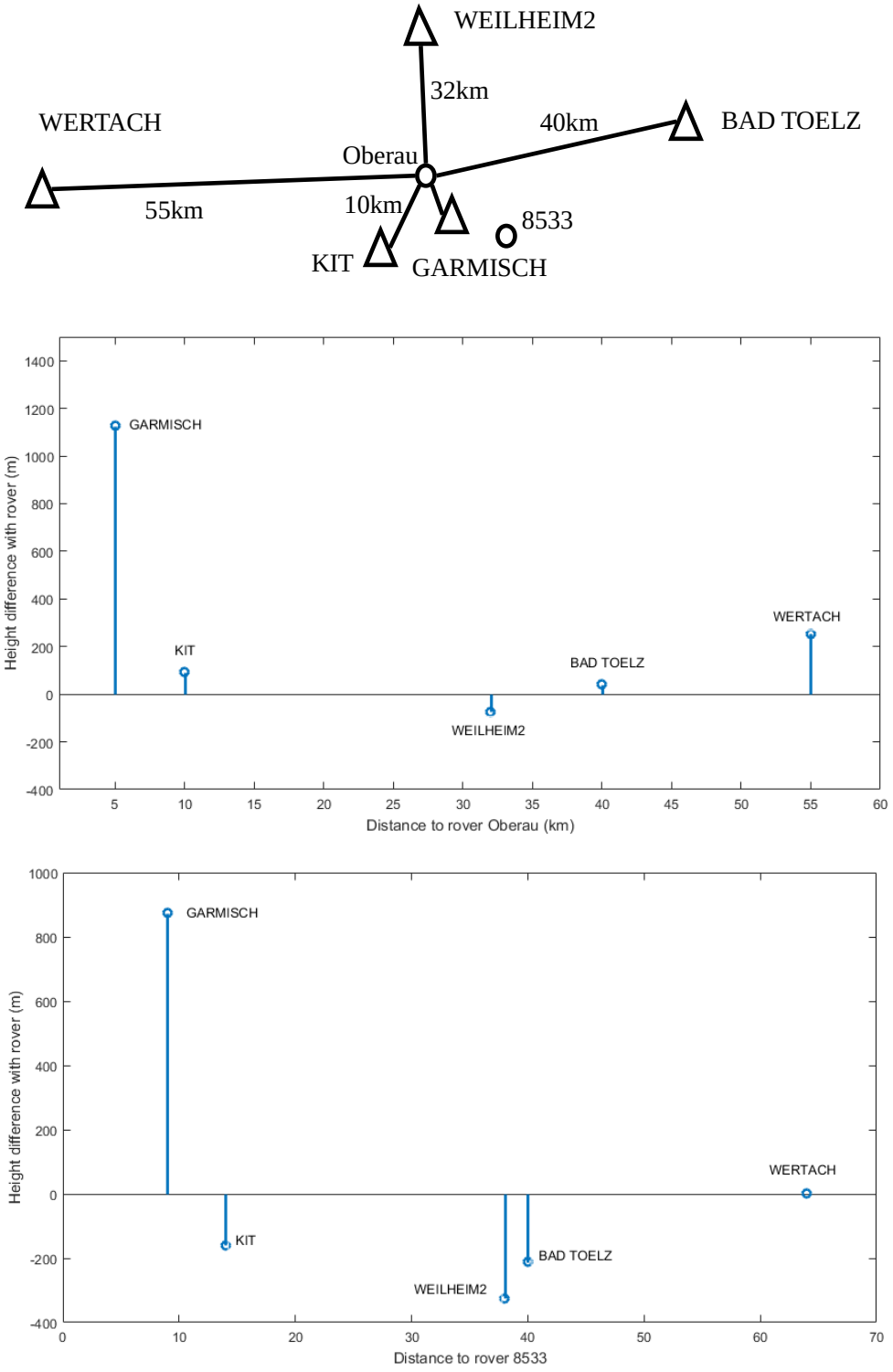

Figure 4.10 Network configuration 2

The LSC is chosen as a representative due to its best performance demonstrated previously. Then the corresponding experiments are conducted with excluding KIT or not. The ZWD interpolation errors of two rovers are depicted in Figure 4.11.

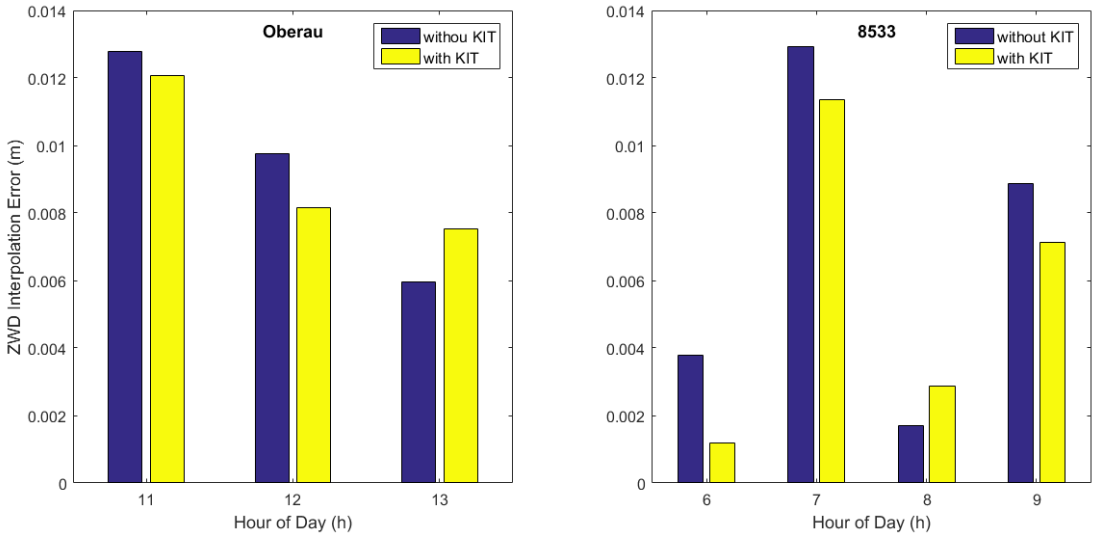

Figure 4.11 ZWD interpolation error with KIT or not

It is clear that the ZWD interpolation could reach centimeter accuracy in both cases, and the maximum is a little bigger than 1cm. It seems the KIT has improvement to some extent due to its closer distance to the rovers, but the improvement is not so significant since the differences of interpolation errors are within millimeter level, which means the limited benefits for height component positioning, which is validated by Figure 4.12. It is indicated that under normal weather conditions, as for a small network with average baseline of 40km, the spatial correlation still maintains and adding reference stations is not critical for improvement. Also, the main statistics of height errors is listed in Table 4.9.

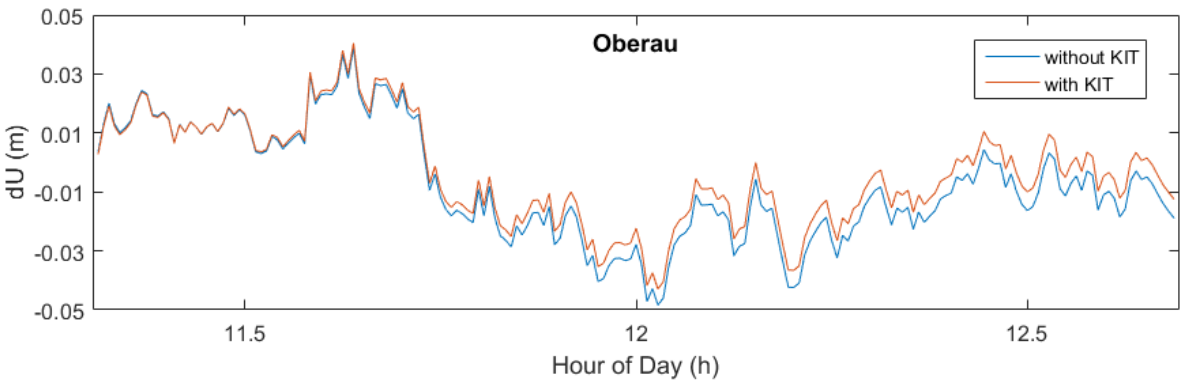

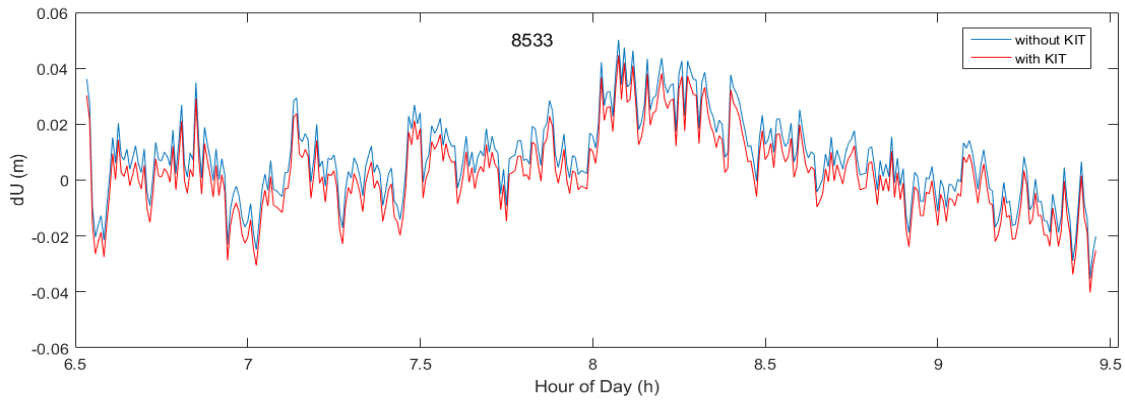

Figure 4.12 Height errors with KIT or not

Table 4.9 Main statistics of height error with or without KIT (cm)

	Oberau		8533	
	with KIT	without KIT	with KIT	without KIT
MAX	4.37	4.53	4.47	5.02
AVG	-0.07	-0.46	0.30	0.87
RMS	1.73	1.95	1.42	1.63

4.4.2 Baseline of Reference Stations

The effective coverage of reference network is determined by the spatial correlation. It is noted that a small network with 40km baseline could reach centimeter level interpolation accuracy. Now the network would be expanded to a medium one with average 80km baseline, in order to investigate the baseline influence.

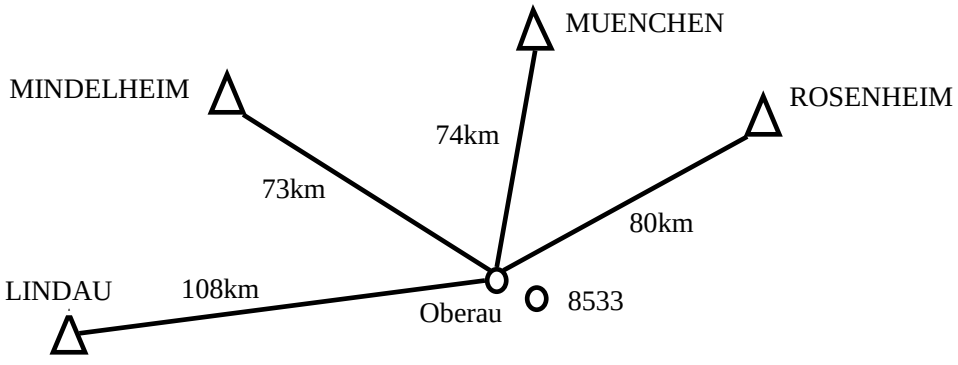

Figure 4.13 Network configuration 3

In Figure 4.14, the ZWD interpolation errors form the medium network are compared with the small network ones obtained in previous part. And Table 4.10 gives the statistics of height error. With the increasing of baseline to nearby reference stations, the performance of ZWD interpolation largely degrades due to the spatial decorrelation effect by distance. The maximum error jumps up to 5cm, compared with 1cm level of small network. Hence, it is always advisable to employ a smaller network.

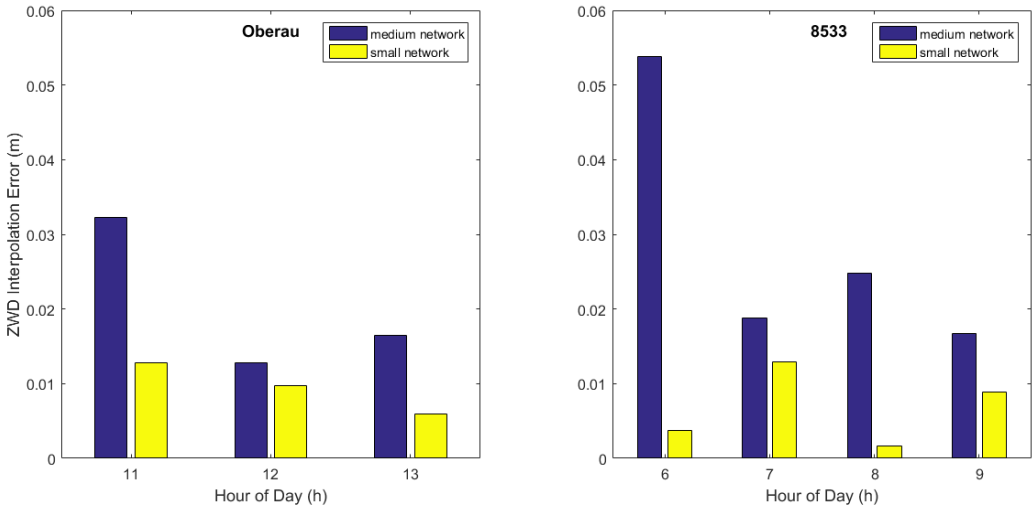

Figure 4.14 ZWD interpolation error of medium and small network

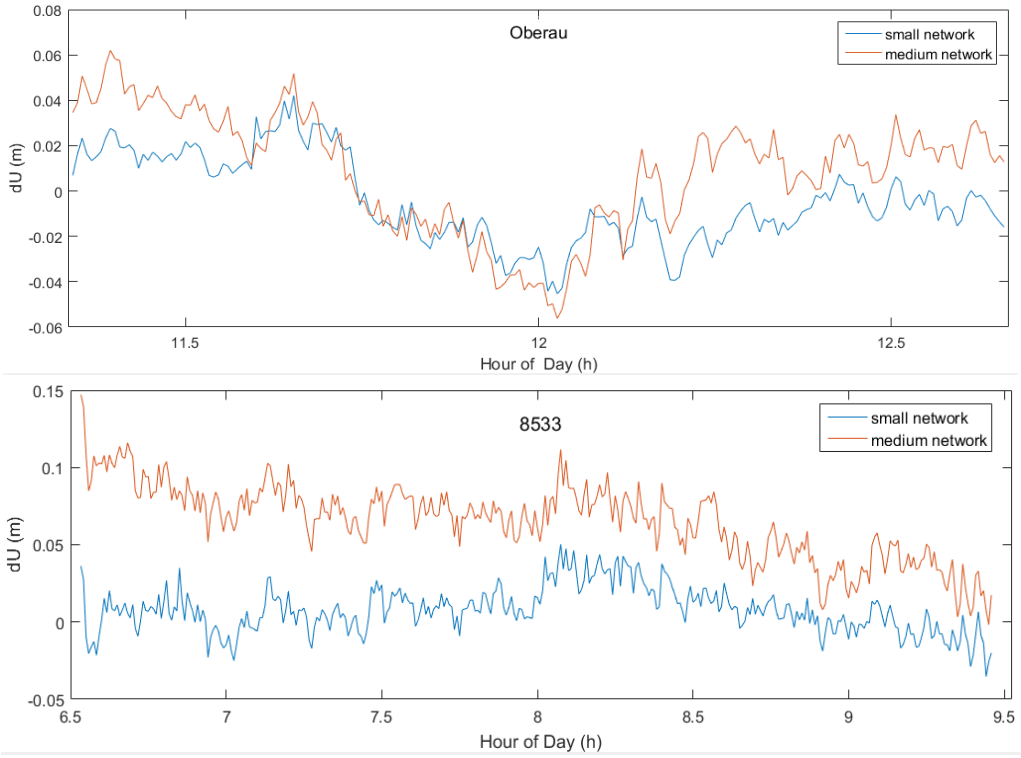

Figure 4.15 Height errors of medium and small network

Table 4.10 Main statistics of height error of medium and small network (cm)

	Oberau		8533	
	medium network	small network	medium network	small network
MAX	6.20	4.37	14.71	4.47
AVG	0.89	-0.07	6.51	0.30
RMS	2.76	1.73	6.95	1.42

4.4.3 Height Distribution of Reference Stations

The ZWD at the reference stations are in essence spatial sampling data at different height and horizontal positions. If the rover is within the height range of the reference stations, the prediction of its ZWD is an interpolation process. All the previous investigations are the interpolation process. If the rover is outside the height range, the prediction is defined as an extrapolation process. It is questionable that the outside boundary points still follow the same spatial pattern. For giving an answer, the reference station with lowest altitude (628m), WEILHEIM2, is chosen as rover. And other reference stations are used to extrapolate the ZWD. Comparisons are made with the interpolation cases, Oberau and 8533, illustrated in Figure 4.16.

It is nice to find that the extrapolation and interpolation cases have only millimeter level difference of errors, which suggests the same spatial pattern still holds for a rover outside the reference height range.

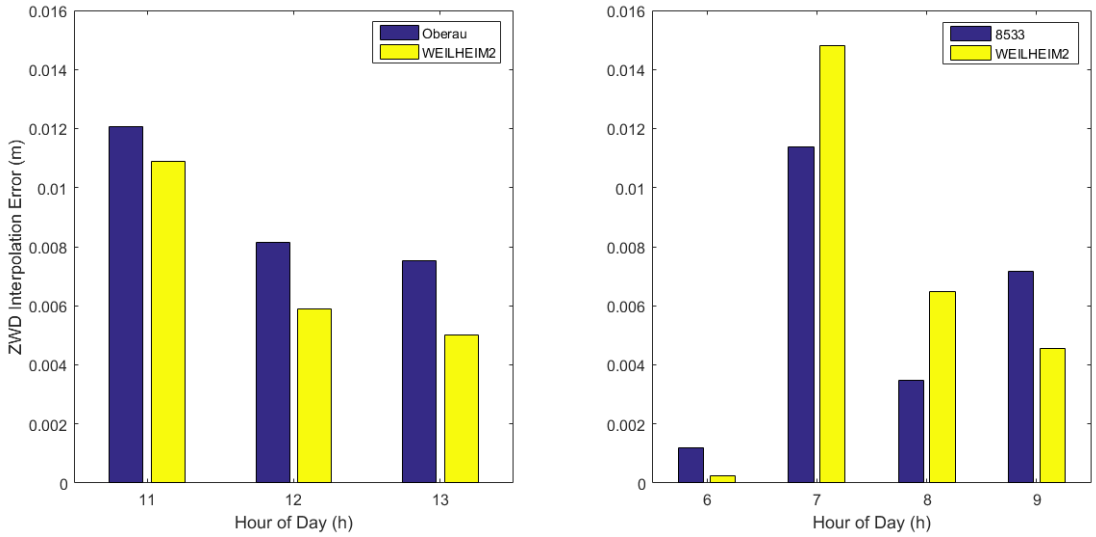

Figure 4.16 ZWD interpolation error of interpolation and extrapolation process

Chapter 5 Conclusions and Outlook

The tropospheric delay remains one of the major error sources in high precision GNSS positioning, especially the ZWD still remaining after empirical models correction. The ZWD has great variability in space and time. But for a local area, there exist spatial correlations within the ZWD. Therefore, it is feasible to establish a local interpolation model for tropospheric delay mitigation. And this is actually one of the core parts of Network RTK technique, in which reference stations are used to resolve the site-specific tropospheric errors and thus fitting a local model.

In this thesis, the emphasis is laid on the error modeling for the mountainous areas where large height difference exists between reference station and rovers, taking the Garmisch-Patenkirchen area as a case. Various models are evaluated and the LSC and HHD outperforms the conventional ones by introducing height correlated function models. The interpolation accuracy could reach at centimeter level for a small network with around 40km baseline under normal weather conditions and hence improve the height component positioning. As for an expanded network with about 80km baseline, the interpolation accuracy largely degrades due to the spatial decorrelation. Besides, it is sensible to make an extrapolation for rovers outside the height range of nearby reference stations since the spatial pattern still holds on.

However, the troposphere irregularity is a ubiquitous phenomenon. Short term extreme weather could significantly affect the spatial pattern in a local area and lead to degraded accuracy of interpolation. A solution could be densification of the reference network thus the denser sampling of tropospheric delay could acquire the subtle flucuations of local spatial pattern. Actually, in the field of GNSS meteorology, the inter-station distance below 20km is suggested to fulfill the accuracy of precipitable water vapor (PWV) retrieval (Braun et al., 1999).

The major problem accompanied with network densification is the economic problem. The price of geodetic dual-frequency receiver is on the order of 10,000 Euros thus it is impractical to equip such receivers for densification. It is worth to investigate using low cost single-frequency receivers as alternatives. The general strategy is to employ existing sparse network as first level reference stations and

the single-frequency ones for densification as the second level. The first level stations are not only responsible for providing ZTD estimations, but also the ionospheric corrections for the second level ones. Some approaches have been developed for local ionosphere modeling, i.e., the high resolution ionospheric modeling technique (HiRIM - Rocken et al., 2000) and the epoch-differenced ionospheric delay model (SEID - Deng et al., 2009). These two methods are implemented in the PWV retrieval experiment in a hyper dense network (1-2km spacing) in Kyoto University (Sato et al., 2013). It seems promising to adopt it in the Network RTK technique to deal with the troposphere irregularity.

Bibliography

Boehm J, Schuh H. Vienna Mapping Functions in VLBI Analyses [J]. Geophysical Research Letters, 2004, 31(1).

Böhm J, Niell A, Tregoning P, et al. Global Mapping Function (GMF): A New Empirical Mapping Function Based on Numerical Weather Model Data [J]. Geophysical Research Letters, 2006, 33(7).

Braun J, Rocken C, Meertens C, et al. Development of A Water Vapor Tomography System using Low Cost L1 GPS Receivers [C]. Proc., Ninth Anrruai ARM Science Team Meeting. 1999.

Dach, R., Hugentobler, U., Fridez, P., and Meindl, M.: Bernese GPS Software Version 5.0 [M], Astronomical Institute, University of Berne, Switzerland, 2007

Darbeheshti N. Modification of the Least-squares Collocation Method for Non-stationary Gravity Field Modelling [D]. Curtin University of Technology, 2009.

Deng Z, Bender M, Dick G, et al. Retrieving Tropospheric Delays from GPS Networks Densified with Single Frequency Receivers [J]. Geophysical Research Letters, 2009, 36(19).

Fotopoulos G, Cannon M E. An Overview of Multi-reference Station Methods for cm-level Positioning[J]. GPS solutions, 2001, 4(3).

Gao Y, Li Z, McLellan J F. Carrier phase based regional area differential GPS for decimeter-level positioning and navigation [C]. Proc. ION GPS-97, 10th International Technical Meeting of the Satellite Division of the US Institute of Navigation). 1997.

Goad C, Goodman L. Modified Hopfield Tropospheric Refraction Correction Model [C]. Transactions-American Geophysical Union. 2000 Florida AVE NW, Washington, DC 20009: AMER GEOPHYSICAL UNION, 1974, 55(12).

Han S, Rizos C. GPS Network Design and Error Mitigation for Real-time Continuous Array Monitoring Systems[C]. Proc. ION GPS-96, 9th International Technical Meeting of the Satellite Division of the US Institute of Navigation. 1996.

Hofmann W B, Lichtenegger H, Collins J. Global Positioning System: Theory and Practice [M]. Springer-Verlag, 2001.

Hopfield H S. Two-quartic Tropospheric Refractivity Profile for Correcting Satellite Data [J]. Journal of Geophysical research, 1969, 74(18).

BIBLIOGRAPHY

Hurter F P. GNSS Meteorology in Spatially Dense Networks [D]. Zürich Eidgenössische Technische Hochschule, 2014.

Lachapelle G, Alves P. Multiple Reference Station approach: Overview and Current Research [J]. Positioning, 2009, 1(02).

Marini J W. Correction of Satellite Tracking Data for an Arbitrary Tropospheric Profile [J]. Radio Science, 1972, 7(2).

Moritz H. Advanced Least-squares Methods[M]. Columbus: Department of Geodetic Science, Ohio State University, 1972.

Niell A E. Global Mapping Functions for the Atmosphere Delay at Radio Wavelengths [J]. Journal of Geophysical Research: Solid Earth, 1996, 101(B2).

Parkinson B W. Progress in Astronautics and Aeronautics: Global Positioning System: Theory and Applications [M]. Aiaa, 1996.

Rizos C, Han S, Chen H. Regional-Scale Multiple Reference Stations for Real-time Carrier PhaseBased GPS Positioning: A Correction Generation Algorithm. Pres [C]. Int. Symp. On GPS: Application to Earth Sciences & Interaction with Other Space Geodetic Techniques. 1999.

Rocken C, Johnson J M, Braun J J, et al. Improving GPS Surveying with Modeled Ionospheric Corrections [J]. Geophysical Research Letters, 2000, 27(23).

Saastamoinen J. Contributions to the Theory of Atmospheric Refraction [J]. Bulletin Géodésique (1946-1975), 1973, 107(1).

Sato K, Realini E, Tsuda T, et al. A High-resolution, Precipitable Water Vapor Monitoring System Using a Dense Network of GNSS Receivers [J]. 2013.

Seeber G. Satellite Geodesy: Foundations, Methods, and Applications [M]. Walter de Gruyter, 2003.

Troller, M. GPS based Determination of the Integrated and Spatially Distributed Water Vapor in the Troposphere[D], Zürich Eidgenössische Technische Hochschule, 2004.

Wanninger L. Improved Ambiguity Resolution by Regional Differential Modelling of the Ionosphere [C]. ION GPS-95. 1995.

Xu G. GPS: Theory, Algorithms and Applications [M]. Springer Science & Business Media, 2007.

Atmosphere of Earth. (n.d.). In Wikipedia. Retrieved March 16, 2016, from https://en.wikipedia.org/

BIBLIOGRAPHY

wiki/Atmosphere_of_Earth.

Troposphere. (n.d.). In Wikipedia. Retrieved March 16, 2016, from https://en.wikipedia.org/wiki/ Tro posphere

Network RTK. (n.d.). In SmartNet. Retrieved March 18, 2016, from http://uk.smartnet-eu.com/netwo rk-rtk_221.htm